

Alma Mater Studiorum Università di Bologna
Archivio istituzionale della ricerca

Design, synthesis and evaluation of novel feruloyl-donepezil hybrids as potential multitarget drugs for the treatment of Alzheimer's disease

This is the final peer-reviewed author's accepted manuscript (postprint) of the following publication:

Published Version:

Dias, K.S.T., de Paula, C.T., dos Santos, T., Souza, I.N.O., Boni, M.S., Guimarães, M.J.R., et al. (2017). Design, synthesis and evaluation of novel feruloyl-donepezil hybrids as potential multitarget drugs for the treatment of Alzheimer's disease. EUROPEAN JOURNAL OF MEDICINAL CHEMISTRY, 130, 440-457 [10.1016/j.ejmech.2017.02.043].

Availability:

This version is available at: <https://hdl.handle.net/11585/623951> since: 2019-05-06

Published:

DOI: <http://doi.org/10.1016/j.ejmech.2017.02.043>

Terms of use:

Some rights reserved. The terms and conditions for the reuse of this version of the manuscript are specified in the publishing policy. For all terms of use and more information see the publisher's website.

This item was downloaded from IRIS Università di Bologna (<https://cris.unibo.it/>).
When citing, please refer to the published version.

(Article begins on next page)

This is the final peer-reviewed accepted manuscript of:

Dias, K. S. T.; de Paula, C. T.; dos Santos, T.; Souza, I. N. O.; Boni, M. S.; Guimarães, M. J. R.; da Silva, F. M. R.; Castro, N. G.; Neves, G. A.; Veloso, C. C.; Coelho, M. M.; de Melo, I. S. F.; Giusti, F. C. V.; Giusti-Paiva, A.; da Silva, M. L.; Dardenne, L. E.; Guedes, I. A.; Pruccoli, L.; Morroni, F.; Tarozzi, A.; Viegas, C. Design, Synthesis and Evaluation of Novel Feruloyl-Donepezil Hybrids as Potential Multitarget Drugs for the Treatment of Alzheimer's Disease. *European Journal of Medicinal Chemistry* **2017**, *130*, 440–457.

The final published version is available online at:

<https://doi.org/10.1016/j.ejmech.2017.02.043>.

Rights / License:

The terms and conditions for the reuse of this version of the manuscript are specified in the publishing policy. For all terms of use and more information see the publisher's website.

This item was downloaded from IRIS Università di Bologna (<https://cris.unibo.it/>)

When citing, please refer to the published version.

Design, synthesis and evaluation of novel feruloyl-donepezil hybrids as potential multitarget drugs for the treatment of Alzheimer's disease

Kris Simone T. Dias ^a, Cynthia T. de Paula ^a, Thiago dos Santos ^a, Isis N. O. Souza ^b, Marina S. Boni ^b, Marcos J. R. Guimarães ^b, Fernanda M. R. da Silva ^b, Newton G. Castro ^b, Gilda Neves ^b, Clarice C. Veloso ^c, Márcio M. Coelho ^d, Ivo Souza F. de Melo ^d, Fabiana C. Vilela^e, Alexandre Giusti-Paiva ^e, Marcelo L. da Silva ^f, Laurent E. Dardenne ^g, Isabella Guedes ^g, Letizia Pruccoli ^h, Fabiana Morroni ⁱ, Andrea Tarozzi ^h and Claudio Viegas Jr.^a

^a PeQuiM- Laboratory of Research in Medicinal Chemistry, Institute of Chemistry, Federal University of Alfenas, 37130-000, Alfenas/MG, Brazil

^b Laboratory of Molecular Pharmacology, Institute of Biomedical Sciences, Federal University of Rio de Janeiro, 21941-902, Rio de Janeiro/RJ, Brazil

^c Pharmaceutical Sciences Faculty, Federal University of Amazonas (UFAM), 69067-005, Manaus/AM, Brazil

^d Department of Pharmaceutical Products, Pharmaceutical Faculty, Federal University of Minas Gerais, 31270-901, Belo Horizonte/MG, Brazil

^e Department of Physiological Sciences, Federal University of Alfenas, 37130-000, Alfenas/MG, Brazil

^f Physiotherapy Department, Federal University of Alfenas, 37130-000, Alfenas/MG, Brazil

^g National Laboratory of Scientific Computation, 25651-075, Petrópolis/RJ, Brazil

^h Department for Life Quality Studies, Alma Mater Studiorum-University of Bologna, 47921 Rimini, Italy

ⁱ Department of Pharmacy and Biotechnology, Alma Mater Studiorum-University of Bologna, 40126 Bologna, Italy

*Corresponding author: Claudio Viegas Jr.

Phone: +55 35 37011880

e-mail: cvjviegas@gmail.com

ABSTRACT

A novel series of feruloyl-donepezil hybrid compounds were designed, synthesized and evaluated as multitarget drug candidates for the treatment of Alzheimer's Disease (AD). *In vitro* results revealed potent acetylcholinesterase (AChE) inhibitory activity for some of these compounds and all of them showed moderate antioxidant properties. Compounds **12a**, **12b** and **12c** were the most potent AChE inhibitors, highlighting **12a** with $IC_{50} = 0.46 \mu M$. In addition, these three most promising compounds exhibited significant *in vivo* anti-inflammatory activity in the mice paw edema, pleurisy and formalin-induced hyperalgesy models, *in vitro* metal chelator activity for Cu^{2+} and Fe^{2+} , and neuroprotection of human neuronal cells against oxidative damage. Molecular docking studies corroborated the *in vitro* inhibitory mode of interaction of these active compounds on AChE. Based on these data, compound **12a** was identified as a novel promising drug prototype candidate for the treatment of AD with innovative structural feature and multitarget effects.

Key words: feruloyl-donepezil hybrids, Alzheimer's Disease, multitarget-directed ligands

1. INTRODUCTION

Alzheimer's disease (AD) is a progressive neurodegenerative condition, characterized by cognitive impairment and behavioral abnormalities [1]. In the late stage of the disease, patients lose their personal independence, requiring daily familiar and nursing care, progressing to death. AD is a multifactorial disease, with several interconnected neuropathological events, probably as a result of the combination of risk factors, including age, genetic and environmental factors [2]. It is estimated that more than 18 million people are currently affected by AD worldwide, with an expected increase of patient numbers to 114 million by 2050 [3]. The pathophysiology of AD is not completely understood, but much progress has been achieved in recent years in unveiling the mechanisms of neurodegeneration, given the importance of this disease on the world scene. AD's pathogenesis involves imbalance in numerous biochemical pathways such as the production and clearance of β -amyloid ($A\beta$) peptides, accumulation of hyperphosphorylated tau protein [4–6], decrease in brain acetylcholine (ACh) levels [7,8], dyshomeostasis of biometals such as Zn^{2+} , Fe^{2+} , Cu^{2+} [9,10], oxidative stress and mitochondrial dysfunction [11], and neuroinflammation [12], leading to neuronal damage and death.

Currently, most of the approved drugs for AD treatment are acetylcholinesterase (AChE) inhibitors (e.g. donepezil (1), tacrine (2), rivastigmine (3) and galantamine (4) Fig. 1). Such drugs restore cognitive function and hence improve the quality of life of AD patients [8].

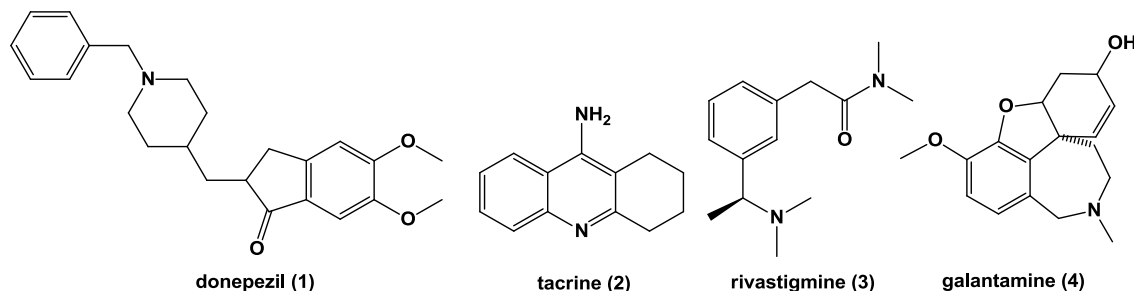


Fig. 1. Chemical structures of AChE inhibitors currently used in the treatment of AD

It has now been accepted that complex multifactorial diseases, such as cancer, diabetes, hypertension and neurodegenerative diseases, cannot be efficiently treated by the

modulation of a single target. As a consequence, the multi-target-directed ligand (MTDL) approach has emerged as a new paradigm in drug discovery. This innovative strategy proposes the design of new scaffolds with two or more pharmacophoric subunits connected in a single molecule that could, in turn, modulate the interaction and biological response of multiple molecular targets simultaneously [13–15].

Considering the MTDLs concept, donepezil, the current first choice drug for AD treatment, is among the most popular pharmacophore inspirations used for the design of novel drug candidates, since it is a very potent, low toxic and well tolerated AChE inhibitor [16–19]. Curcumin (**5**, **Fig.2**), an abundant natural polyphenol found in *Curcuma longa* rhizomes, is also widely used as scaffold for the planning of new MTDLs for AD [20–24]. Curcumin has potent antioxidant and anti-inflammatory properties, playing an important role in the decrease of oxidative damage, inflammation [25,26] and amyloid accumulation [27], with an additional biometal chelating ability [28]. *In vivo* studies with curcumin on transgenic animal models have disclosed its various beneficial effects for the treatment of AD. These studies demonstrate that **5** is also capable of reverting the formation of amyloid plaques, preventing A β -induced oxidative stress, and modulating the expression of inflammatory mediators [29].

Based on the MTDL strategy, we report here the design, synthesis and pharmacological evaluation of a new series of molecular hybrids feruloyl-donepezil based on the combination of the pharmacophoric N-benzylpiperidine, subunit from donepezil (**1**) responsible for its adequate recognition by AchE and the subunit feruloyl present in ferulic acid (**6**) and curcumin (**5**) (**Fig. 2**). Variation of the substituent groups in the aromatic rings moiety derived from donepezil and feruloyl aimed structure-activity relationship (SAR) studies and the identification of potential effective drug candidates for AD treatment, with an innovative mechanism of action.

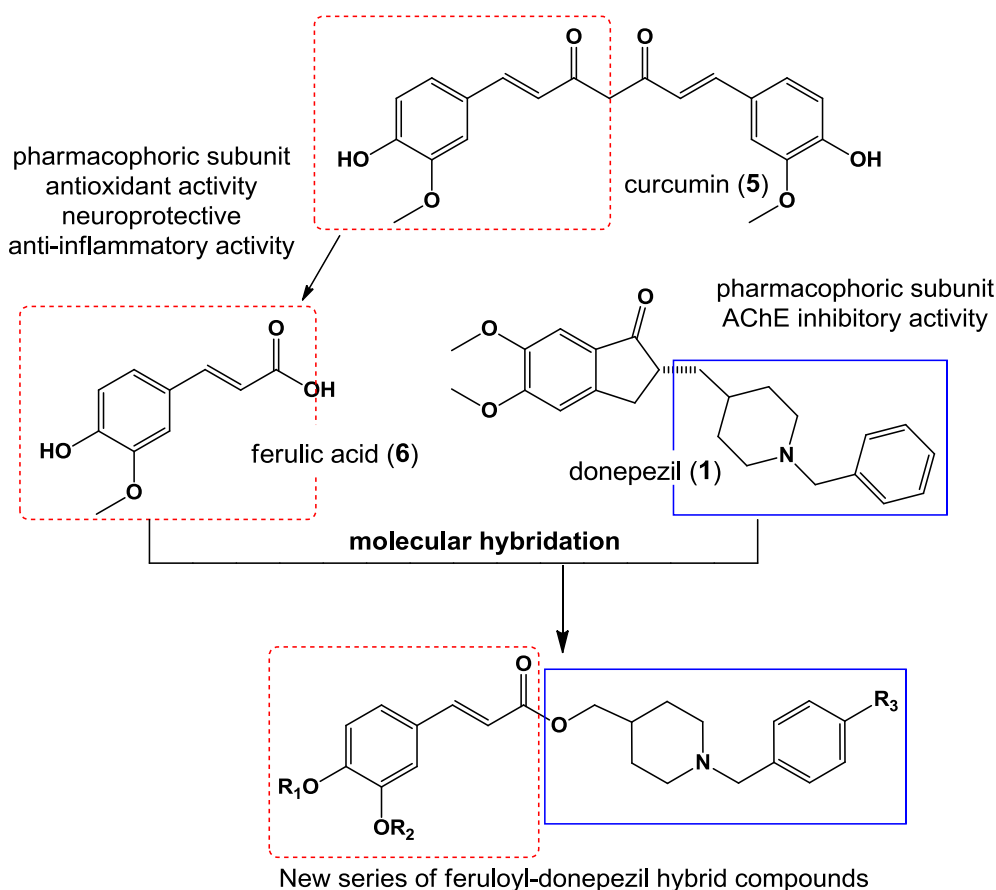


Fig. 2. Design strategy for a new series of feruloyl-donepezil hybrid compounds

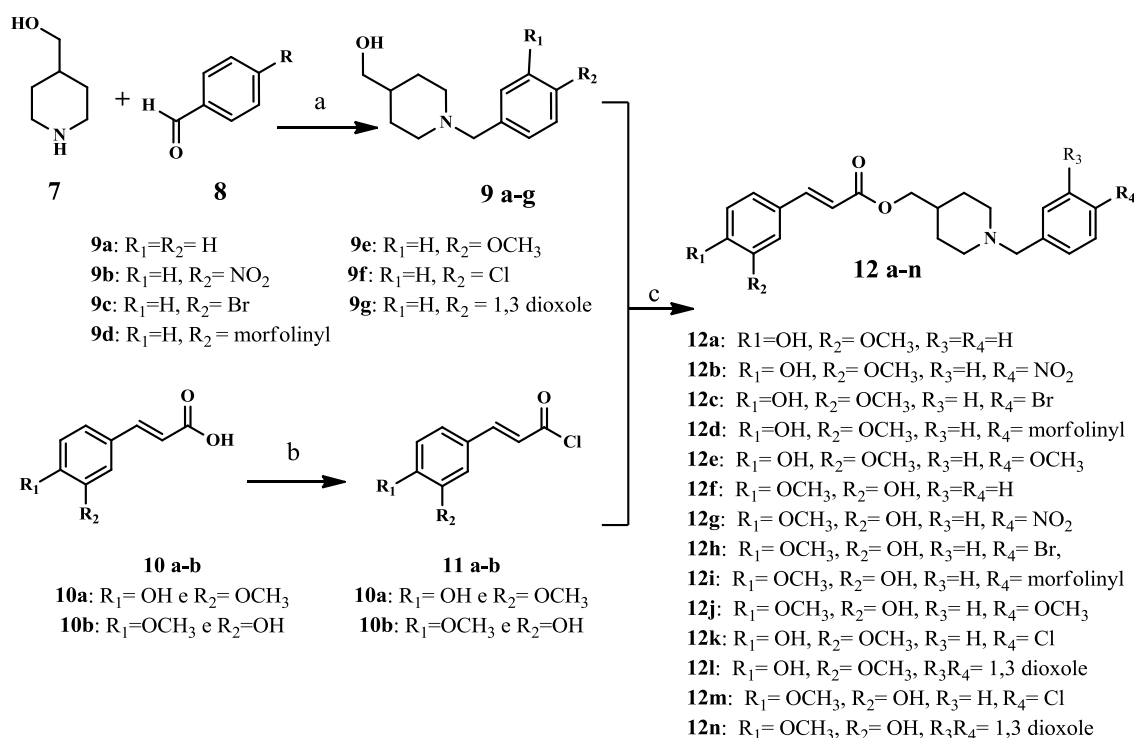
This series of hybrid compounds were investigated for their *in vitro* direct and indirect antioxidant, anticholinesterase, metal chelating and neuroprotective properties, and *in vivo* anti-inflammatory effects. In addition, molecular docking studies were performed to determine the binding mode of the best AChE inhibitors.

2. RESULTS AND DISCUSSION

2.1. Chemistry

The synthetic convergent route for accessing the desired compounds **12a-n** is shown in Scheme 1. 4-piperidinemethanol (**6**) was used as starting material for the preparation of the key intermediates **9a-g**, by a reductive amination reaction with a series of functionalized benzaldehydes in the presence of $\text{NaBH}_3\text{CN}/\text{ZnCl}_2$. Thereafter, ferulic acid (**9a**) and *iso*-ferulic acid (**9b**) were converted into their acyl-chloride derivatives **10a-b** by using thionyl chloride. In a final step, derivatives **10a** and **10b**

were coupled to the *N*-benzylpiperidine key-intermediates **9a-g** to yield the target-compounds **12a-n**.



Scheme 1. Reagents and conditions: (a) NaBH₃CN, ZnCl₂, MeOH, rt, 72 h, 70-87%; (b) SOCl₂, DMF, CH₂Cl₂, N₂, 1h, 98%; (c) CH₂Cl₂, N₂, 15 min, rt, 55-70%

2.2. *In vitro* AChE activity inhibition

Firstly, all feruloyl-donepezil hybrids compounds (**12a-n**) were screened for their cholinesterase inhibition profile on *Electrophorus electricus* AChE (EeAChE), at the fixed concentration of 30 μM. As shown in **Fig. 3**, **12a**, **12b** and **12c** were the most potent AChE inhibitors. However, only compounds **12a** and **12b** reached 50% inhibition, and their IC₅₀ and selectivity versus equine serum butyrylcholinesterase (eqBuChE) were determined next. The unsubstituted benzylpiperidine compound **12a** showed a submicromolar IC₅₀ value for EeAChE (0.46 μM) and marked selectivity, being 53-fold less potent for eqBuChE (**Fig. 4** and **Table 1**). Compound **12b** was about 30-fold less potent than **12a** for EeAChE and only inhibited eqBuChE by 4.3% at 30 μM, so it was not further investigated. Curcumin (**5**) showed only a minor anticholinesterase activity, which is unlikely to contribute to its biological effects *in*

vivo. In the substrate competition assay for EeAChE, compound **12a** reduced V_{\max} without affecting the apparent K_m , therefore indicating a simple (pure) non-competitive inhibition, with a K_i of 1.04 μM (**Fig. 4**). The reference compound donepezil (**1**) also had no discernible effect on the apparent K_m , showing a single K_i of 38 nM. These results suggested that the regiochemistry of the hydroxy and methoxy substituents on the phenylpropanoid moiety is a strong determinant of AChE inhibitory activity, as could be observed for the most active ferulic acid derivatives in comparison to all their regioisomers derived from *iso*-ferulic acid. In addition, the higher potency of compound **12a** suggests that substitution on the aromatic ring of the *N*-benzylpiperidine subunit leads to a decrease in the AChE inhibitory activity, independent of its size or electron donating or withdrawing ability.

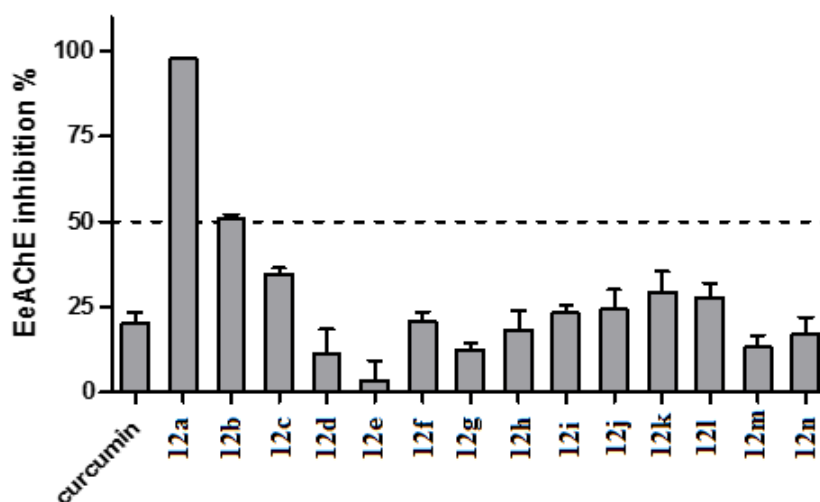


Fig. 3. Screening of feruloyl-donepezil hybrids (**12a-12n**) for EeAChE inhibition. The compounds were pre-incubated for 10 min with the enzyme and reaction was followed for 5 min and activity (velocity) was expressed as percent of control (vehicle). Data are means and pooled SD from 2-4 experiments, each performed in triplicate.

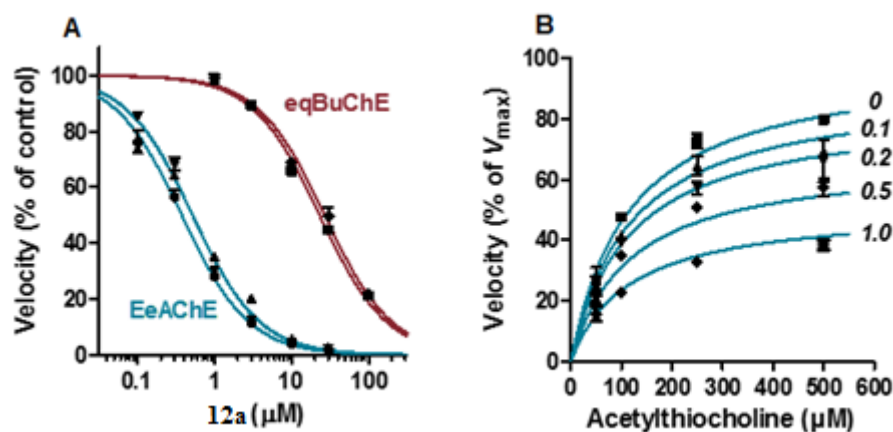


Fig. 4. Inhibition curves and mechanism of inhibition of **12a**. **A.** Concentration-dependent inhibition of EeAChE and eqBuChE by **12a**. Independent experiments are shown in different symbols, which are mean \pm SD of triplicates; fitted curve parameters are shown in Table 2. **B.** Substrate competition data for EeAChE and best-fitting model (simple linear non-competitive inhibition). The concentration of **12a** (μ M) is indicated to the right of each curve. Data are pooled from two experiments, each performed in triplicate.

Table 1. Cholinesterase inhibitory activity, DPPH scavenging capacity, neurotoxic and direct antioxidant effects in neuron cells of compounds **12a-n**

Compounds	Cholinesterase		DPPH	Neuron	Neurotoxicity
	inhibitor IC ₅₀ (μ M) ^a		scavenging	Antioxidant	IC ₅₀ (μ M) ^d
	EeAChE	eqBuChE	EC ₅₀ (μ M) ^b	effects IC ₅₀ (μ M) ^c	
12a	0.46 (3)	24.97 (2)	49.41	16.87	n.d. ^f (6%) ^g
12b	16.74 (3)	-	46.66	25.94	n.d. (9%)
12c	>30	-	45.38	n.d. ^e	n.d. (28%)
12d	> 30	-	73.77	-	-
12e	> 30	-	78.09	-	-
12f	> 30	-	> 100	-	-
12g	> 30	-	> 100	-	-
12h	> 30	-	> 100	-	-
12i	> 30	-	> 100	-	-
12j	> 30	-	> 100	-	-
12k	> 30	-	20.47	-	-
12l	> 30	-	> 100	-	-
12m	> 30.00	-	12.45	-	-

12n	> 30.00	-	> 100	-	-
Donepezil	0.026 (2)	4.69 (2)	-	n.d.	-
Curcumin	132.13 (3)	>300 (2)	-	-	-
Trolox	-	-	04.86	-	-
ferulic acid	-	-	35.54	11.82	-
iso-ferulic acid	-	-	> 100	-	-

^a The IC₅₀ are geometric means from the number of independent experiments indicated in parenthesis; each was performed in triplicate.

^b Antioxidant activity are shown as EC₅₀ values in μ M concentrations. All compounds were analyzed in triplicate and the results expressed as average

^c Concentration of compound resulting in 50% inhibition of ROS formation induced by H₂O₂ (100 μ M) in neuronal SH-SY5Y cells. The values are mean of at least two independent experiments;

^d Concentration of compound resulting in 50% inhibition of neuronal viability after 24 h treatment;

^e n.d: IC₅₀ not determined because less than 50% inhibition of ROS formation induced by H₂O₂ in neuronal SH-SY5Y cells was observed at the highest concentration tested (40 μ M);

^f n.d: IC₅₀ not determined because less than 50% inhibition of neuronal viability was observed at the highest concentration tested (40 μ M);

^g Values in parenthesis are percent inhibition of neuronal viability observed at highest tested concentration (40 μ M).

2.3. Molecular docking study with human AChE

The compound **12a** exhibited similar binding mode and slightly similar affinity scores in both the free and acetylated forms of the enzyme (**Table 2** and **Fig. 5**), with the scores proving to be slightly better than donepezil. Interestingly, the predicted binding mode for this compound is quite similar to the experimental conformation observed for the AChE-donepezil complex (PDB code 4ey7), retaining several key interactions: (i) the phenyl and the piperidine groups are located in the same region, with the phenyl group making stacking interactions with Trp86 and the piperidine Nitrogen atom interacting with Tyr337 through cation- π and with a water molecule (W931) through a hydrogen bond; (ii) hydrogen bond between the carbonyl of the ester group and the NH main chain of Phe295 (carbonyl group of the indanone ring in donepezil), (iii) stacking interaction between the 2-methoxyphenol ring and the indole system of Trp286 located at the peripheral anionic site (PAS). Additionally, the hydroxyl group of the phenol is located at hydrogen-bond distance from Tyr72 (3.06 Å).

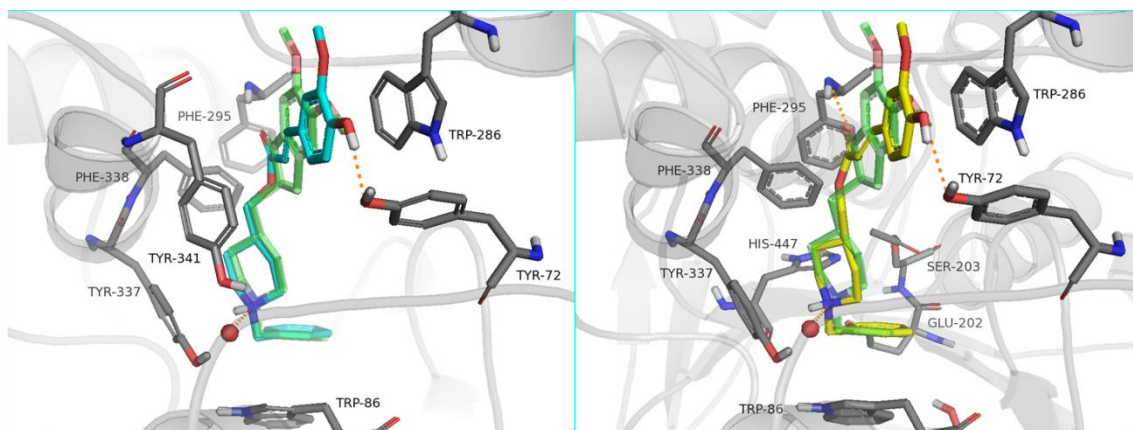


Fig. 5. Docking results for **12a** in the free (light blue) and acetylated (yellow) states, superposed with the experimental binding mode of donepezil (transparent green). W931 is represented as a red sphere and the hydrogen bonds are highlighted as orange dashed lines.

The predicted binding modes of **12b** in the free and acetylated enzyme are also similar, exhibiting the nitrophenyl ring oriented to the catalytic triad (**Table 2** and **Fig. 6**). The main interactions found are: (i) hydrogen bond between the nitro group and the hydroxyl from Tyr133, (ii) salt bridge between nitro and the side chain of Glu202, (iii) stacking interactions between the nitrophenyl ring and Trp86 (not planar) and His447, (iv) cation- π between the NH group in the protonated piperidine and Phe338 (bad geometry), Tyr337 and Trp86 (long distance, $> 6\text{\AA}$), (vi) hydrogen bond between the carbonyl in the ester group with NH of the Phe295 main chain, (vii) stacking interactions between the indanone moiety and Trp286 from PAS (good geometry).

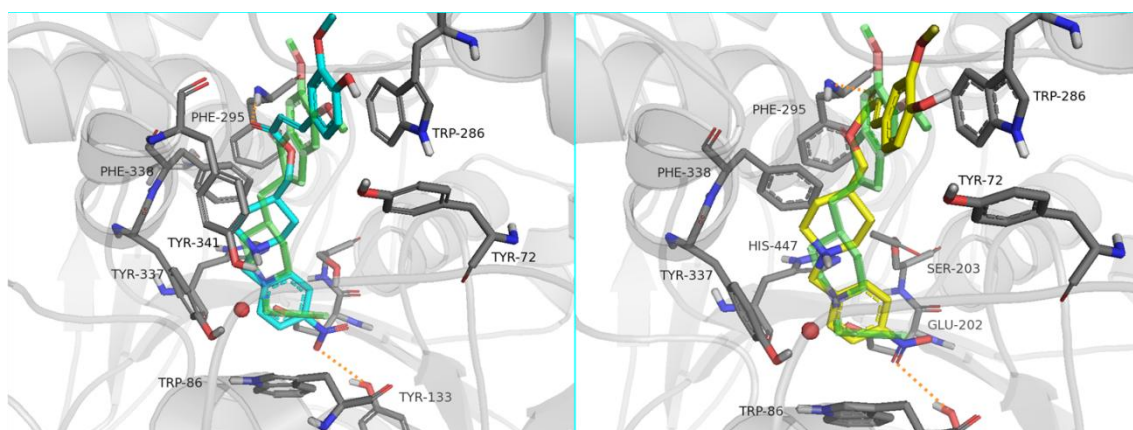


Fig. 6. Docking results for **12b** in the free (light blue) and acetylated (yellow) states, superposed with the experimental binding mode of donepezil (transparent green). W931 is represented as a red sphere and the hydrogen bonds are highlighted as orange dashed lines.

The binding modes of **12c** are significantly similar in both the free and acetylated forms of AChE (**Table 2** and **Fig. 7**), performing similar interactions to those observed for donepezil with some geometry deviations: (i) stacking interactions between the 4-bromine-phenyl ring and Trp86, with the bromine atom oriented to the catalytic triad and surrounded by three structural waters (W731, W722 and W729, not shown), (ii) cation- π between the NH group in the protonated piperidine and Tyr337 and Phe338, (iii) hydrogen bond between the carbonyl in the ester group and the NH of the Phe295 main chain, (iv) stacking interactions with Trp286 from PAS (best interaction in the acetylated form). The significant difference between the scores in the free and acetylated forms (~ 2.6 kcal/mol) might be due to the best geometry of interactions with Trp286 in the PAS (stacking interactions) and with Phe338 (cation- π with the protonated NH oriented to the phenyl ring in the acetylated form while the same group is pointing to the opposite site of the aromatic ring).

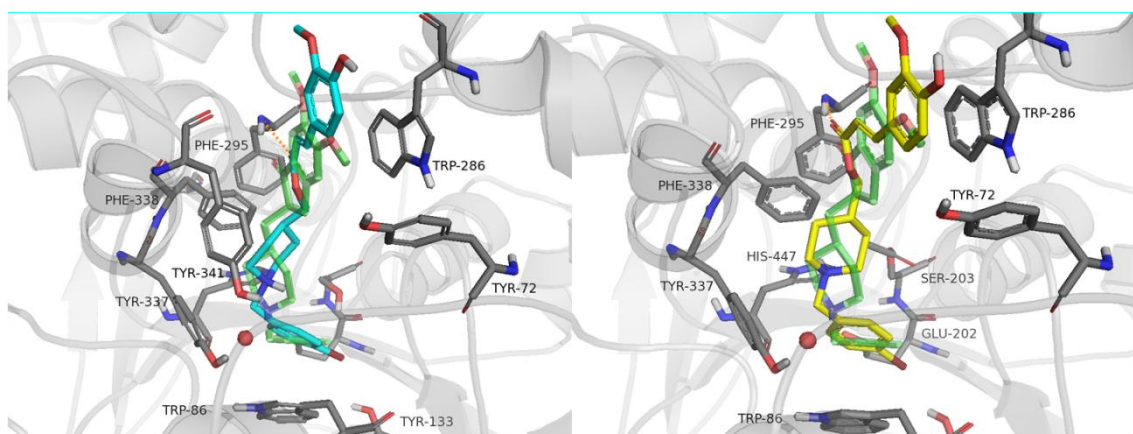


Fig. 7. Docking results for **12c** in the (A) free (light blue) and acetylated (yellow) states, superposed with the experimental binding mode of donepezil (transparent green). W931 is represented as a red sphere and the hydrogen bonds are highlighted as orange dashed lines.

All three compounds exhibited a significant degradation of the docking scores in the Michaelis complex. Compounds **12a** and **12c**, which exhibited the best docking scores, retain the overall orientation in the binding site. On the other hand, compound **12b** exhibited a totally inverted orientation when compared with the predicted binding modes for the free and acetylated enzyme.

Table 2. Docking scores of the compounds **12a**, **12b**, **12c** and donepezil (used as reference) provided by docking with Glide in the Extra Precision Mode.

Compound	Free AChE	Acetylated AChE	Michaelis Complex
12^a	-16.129	-16.956	-11.567
12b	-15.586	-15.982	-9.961
12c	-13.913	-16.566	-11.463
Donepezil	-15.469	-15.862	-11.757

2.4. *In vitro* direct antioxidant activity evaluation

There is ample evidence that oxidative stress plays an important role in inducing and activating multiple cell signaling pathways that contribute to production of toxic substances and then promotes the development of AD [30]. Thereby, compounds **12a-n** were evaluated for their antioxidant activity by using the radical scavenging DPPH assay in different concentrations (12.5, 25, 50, 100 μ M). Ferulic acid, *iso*-ferulic acid and trolox were used as standard compounds and the results are shown in Table 2. It was found that almost all of the ferulic acid related derivatives were effective in scavenging free radicals, in comparison to the *iso*-ferulic parent compounds. Interestingly, ferulic acid exhibited more than 100-fold higher antioxidant potency compared to *iso*-ferulic acid, which revealed that the higher antioxidant profile of compounds **12a-e**, **12k** and **12m** is probably derived from their ferulic acid pattern. These results clearly demonstrate that, similarly to AChE inhibition, regiochemistry plays a key role in the antioxidant activity of the target compounds. This result could be explained by analogy with the effect of *para*-hydroxy substituted cinnamic acids, in which the oxygen atom of the hydroxyl group is able to share a positive charge and thereby increase radical stabilization through conjugation extension. However, if the hydroxyl radicals assume a *meta* orientation, the oxygen atom is unable to share the charge, probably influencing the ability for radical scavenging [31].

We then evaluated the neurotoxic and direct antioxidant effects of compounds **12a**, **12b** and **12c** which showed the best abilities to inhibit the cholinesterase activity and counteract the DPPH radical in neuronal SH-SY5Y cells. As reported in **Table 1**,

treatment for 24 h of SH-SY5Y cells with compounds **12a** and **12b** (1.25-40 μ M) did not affect the neuronal viability using MTT assay, while the similar treatment with compound **12c** showed a slight decrease in neuronal viability (28%) at the highest concentration (40 μ M) used. In parallel, we recorded the strong ability of compounds **12a** and **12b**, but not **12c**, to counteract the intracellular ROS formation induced by H_2O_2 in SH-SY5Y cells using DCFDA probe (**Table 1**). Both compounds **12a** and **12b** showed concentration-dependent antioxidant effects with a significant decrease of ROS formation at 10, 20 and 40 μ M (all $p < 0.001$). Compound **12c** significantly inhibited the ROS formation only at 10 μ M ($p < 0.001$), showing pro-oxidant effects at higher concentrations (**Fig. 8**). Antioxidant profiles similar to those of **12a** and **12b** were recorded with ferulic acid (**Table 1**, **Fig. 8**). As expected, donepezil did not show any direct antioxidant effects (data not shown). These results show the absence of cytotoxic and pro-oxidant effects for compounds **12a** and **12b** and suggest that their ferulic acid pattern effectively contributes to counteract the ROS formation in neuron SH-SY5Y cells.

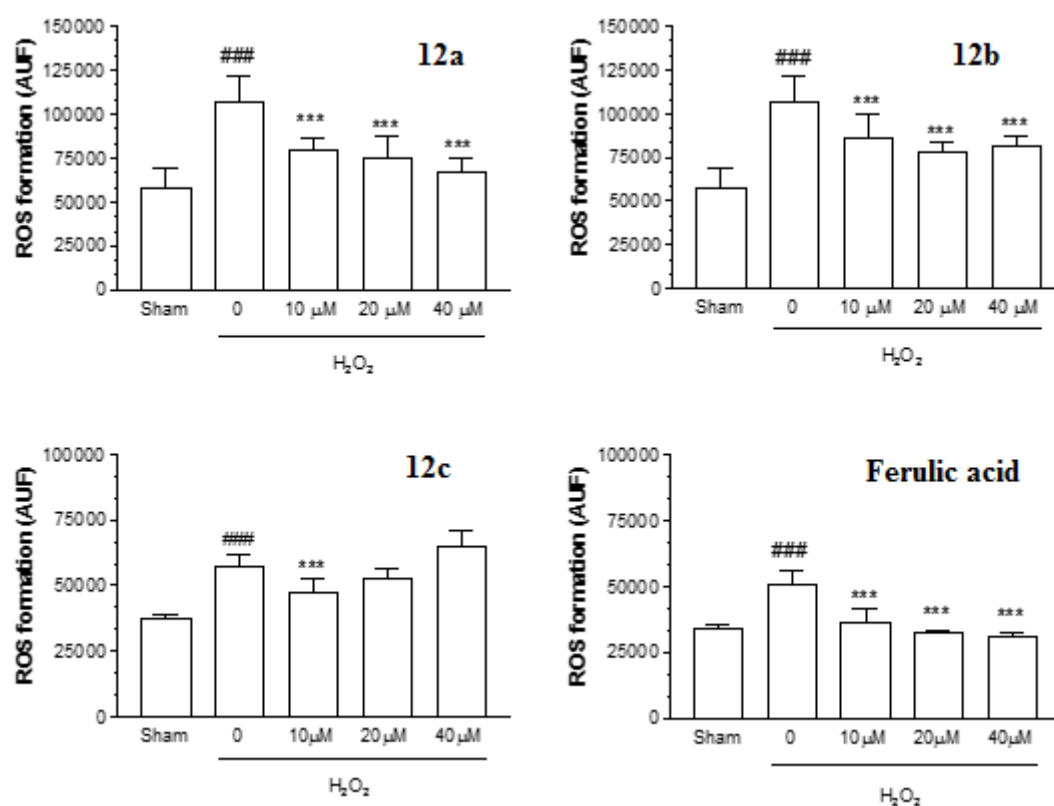


Fig. 8. Compounds **12a**, **12b**, **12c** and ferulic acid counteract the ROS formation induced by H_2O_2 in neuronal SH-SY5Y cells. The cells were treated with various concentrations of

compounds and H_2O_2 (100 μM) for 30 min. At the end of the treatment, intracellular ROS formation was determined using DCFDA probe (as described in the experimental section). The arbitrary units of fluorescence (AUF) values are shown as mean \pm SD of three independent experiments ($^{###}\text{p}<0.001$ vs sham; $^{***}\text{p}<0.001$ vs treated with H_2O_2).

2.5. Chelation of pro-oxidant metals

A considerable amount of literature data has shown that the dyshomeostasis of biometals such as Cu^{2+} , Zn^{2+} , Fe^{2+} and Fe^{3+} in CNS and their interactions with amyloid protein precursor (APP) and $\text{A}\beta$ could contribute to AD pathology [10], [9], [32]. In particular, copper and iron are redox active and can generate ROS via the Fenton and Haber–Weiss reaction, and promote neurotoxic $\text{A}\beta$ oligomer formation. Therefore, compounds with metal-chelating properties could represent an additional therapeutic strategy for the treatment of AD. The ability of compounds **12a-c** to chelate biometals such as Cu^{+2} , Fe^{+2} , Fe^{+3} and Zn^{2+} was studied by UV–vis spectroscopy with wavelengths ranging from 200 to 400 nm, according to the methodology described by Chen and cols. [20]. Compound **12a** selectively chelated copper and iron. The absorption spectra of **12a** at the concentration of 75 μM alone or incubated in the presence of CuSO_4 , FeSO_4 , FeCl_3 or ZnCl_2 (150 μM) for 30 min in ethanol are shown in **Fig. 9**. Compound **12a** displayed absorptions with λ_{max} ($\log \epsilon$) at 328.20 nm (0.970), 299.00 nm (0.660) and 237.20 nm (0.517). When Cu^{2+} was added to the solution of **12a**, it caused a significant shift of the band at 237.20 nm (0.517) to 248.00 nm (0.470), indicating the formation of the corresponding complex via metal chelation. Similarly, after addition of Fe^{2+} , a shift of the band at 237.20 nm (0.517) to 249.20 nm (0.430) was also observed. In contrast, the addition of FeCl_3 and ZnCl_2 did not cause any significant shift in the absorption bands, which confirms that compound **12a** is capable of chelating only Cu^{2+} and Fe^{2+} , but not Fe^{3+} and Zn^{2+} . Compounds **12b** and **12c** showed the same profile as the compound **12a** (data not shown).

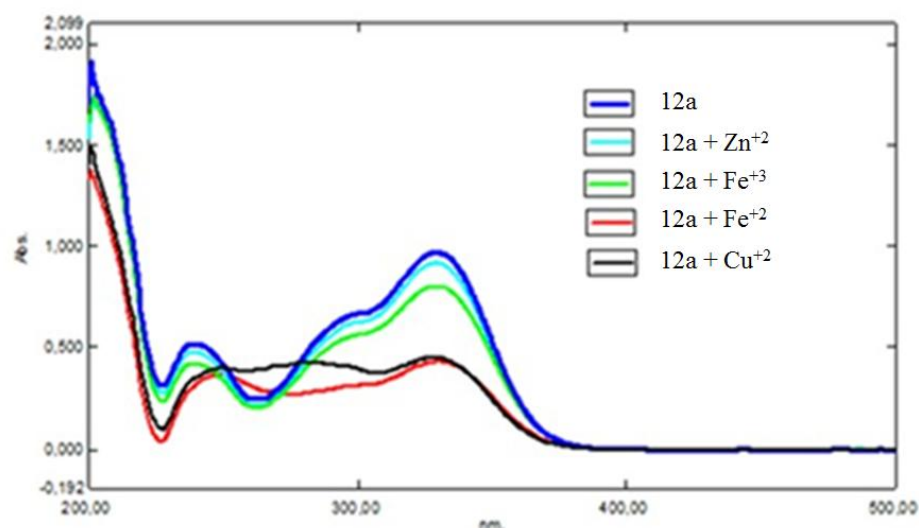


Fig.9. UV-absorbance spectra of **12a** alone or in the presence of ZnCl₂, FeSO₄, FeCl₃ and CuSO₄.

We then determined the ability of compound **12a** to counteract the ROS formation elicited by Fenton reaction with either Cu²⁺ or Fe²⁺ and H₂O₂ in neuronal SH-SH5Y cells. In both the reactions, 5, 10 and 20 μM of compound **12a** significantly counteracted the ROS formation in neuronal SH-SH5Y cells ($p < 0.001$) (**Fig. 10**).

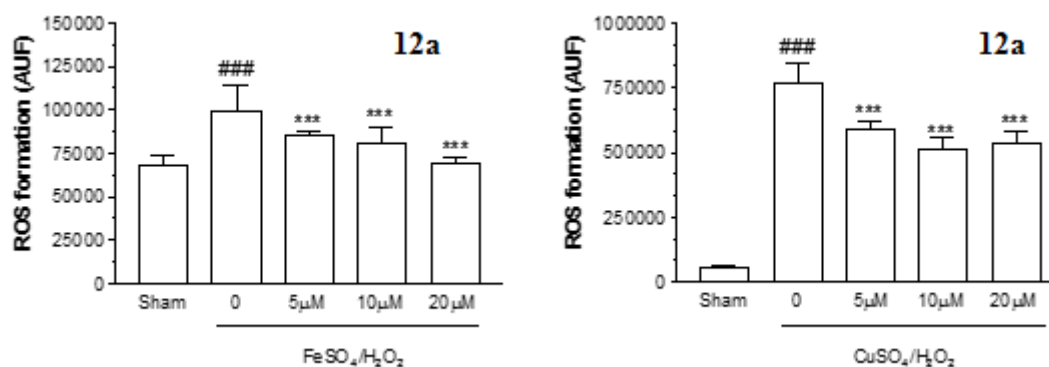


Fig.10. Compound **12a** counteracted the ROS formation induced by either FeSO₄/H₂O₂ or CuSO₄/H₂O₂ in neuronal SH-SY5Y cells. The cells were treated with various concentrations of compound **12a** and either FeSO₄/H₂O₂ or CuSO₄/H₂O₂ (25 μM/100 μM) for 30 min. At the end of the treatment, intracellular ROS formation was determined using DCFDA probe (as described in the experimental section). The arbitrary units of fluorescence (AUF) values are shown as mean ± SD of three independent experiments (### $p < 0.001$ vs sham; *** $p < 0.001$ vs treated with either FeSO₄/H₂O₂ or CuSO₄/H₂O₂).

2.6. *In vitro* indirect antioxidant activity evaluation

Recent studies report that molecules like curcumin which contain Michael acceptor functionalities and phenolic hydroxyl groups with direct antioxidant properties can also induce antioxidant and cytoprotective proteins at cellular level. In particular, these indirect antioxidants activate the Keap1/Nrf2/ARE pathway resulting in transcriptional induction of glutathione (GSH) and Phase II detoxification enzymes that act catalytically (not being consumed and having long half-lives), and are unlikely to evoke pro-oxidant effects [33].

On the basis of these considerations, we determined the intracellular GSH levels after a 24 h treatment of neuronal SH-SH5Y cells with 20 μ M compounds **12a**, **12b** and **12c** using MCB probe. As reported in **Fig. 12a**, compounds **12a**, **12b**, but not **12c**, increased the GSH levels with a maximum of 1.4- and 1.2-fold increase, respectively. Furthermore, compound **12a** induced a time-dependent increase of GSH levels with a maximum of 24-fold increase at 24 h (**Fig. 12b**). We then chose compound **12a** to evaluate its ability to activate Nrf2 binding to ARE at nuclear level, an essential event for the induction of GSH synthetic enzyme genes, by TransAM ELISA kit. At the 20 μ M concentration of **12a** we recorded a strong time dependent increase of nuclear Nrf2 activity starting at 1 h. COS-7 cells transfected with Nrf2 were used as a positive control (**Fig. 12c**). The activity of this positive control showed the reliability of this assay (data not shown). Finally, to ascertain whether the increase of the total GSH level observed in SH-SY5Y cells could really translate into antioxidant effects, we treated the SH-SY5Y cells 24 h before adding the H₂O₂. Remarkably, 20 μ M of compound **12a** significantly prevented the ROS formation evoked by H₂O₂ in SH-SY5Y cells (**Fig. 12d**).

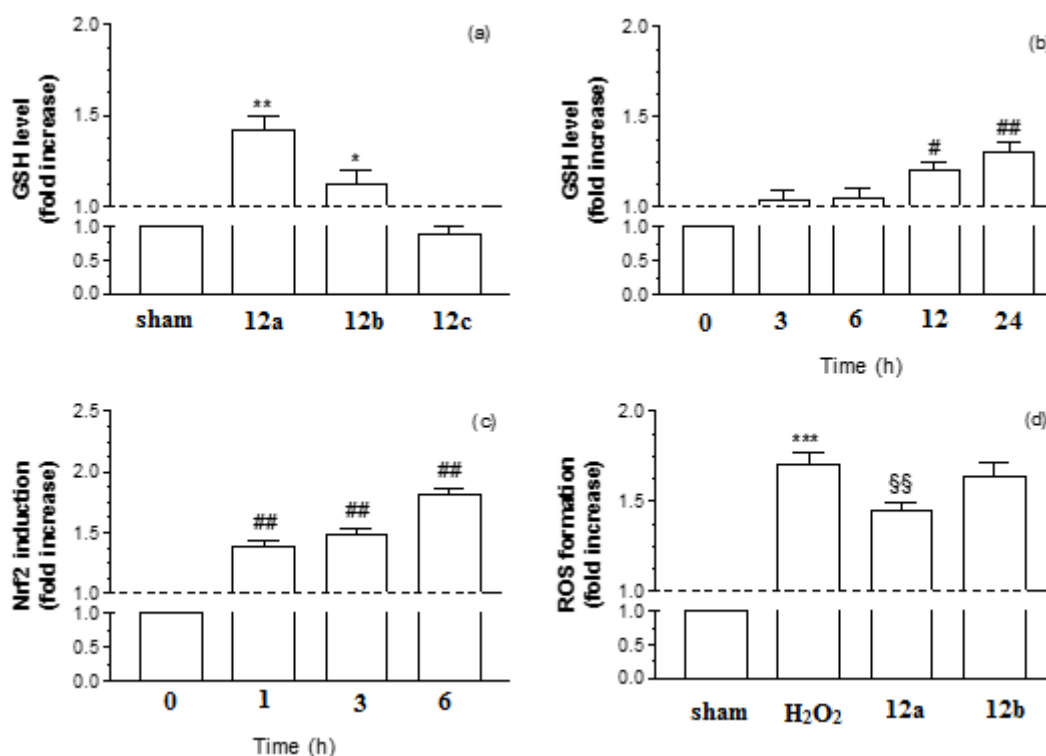


Fig. 11. Compound **12a** increases cytosolic GSH and nuclear Nrf2 levels as well as indirect antioxidant effects in neuronal SH-SY5Y cells. The cells were treated with 20 μ M of compounds **12a**, **12b**, **12c** for 24 h (a) or various increasing treatment time (b, c). At the end of the treatment, cytosolic GSH and nuclear Nrf2 levels were determined using MCB probe and immunoassay, respectively (as described in experimental section). (d) After the 24 h treatment with 20 μ M of compound **12a**, the cells were also treated with H₂O₂ (100 μ M, 30 min) to evaluate the intracellular ROS formation using DCFDA probe (as described in the experimental section) in SH-SY5Y cells. The results are expressed as a percentage of control cells. The values are reported as mean \pm SD of three independent experiments (* p <0.05, ** p <0.01, *** p <0.001 vs sham; # p <0.05, ## p <0.01 vs untreated; §§ p <0.01 vs treated with H₂O₂).

2.7. *In vitro* neuroprotective activity evaluation

Several studies have suggested that A β oligomers cause a selective synaptic dysfunction and/or neuronal loss in cortex and hippocampus, two stricken brain regions in AD [4]. In one proposed mechanism, A β oligomers adhere to the plasma membrane of neurons and cause lesions by a combination of radical species-initiated lipid peroxidation and formation of ion-permeable pores which initiate a cascade of pathological processes that end with neuronal death [34]. We evaluated the ability of

compound **12a** to counteract the ROS formation, early and late neurotoxic events elicited by A β ₁₋₄₂ oligomers. Twenty micromolar of compound **12a** decreased ROS formation elicited by A β ₁₋₄₂ oligomers in neuronal SH-SY5Y cells (**Fig. 12**). In parallel, compound **12a** did not counteract early vacuole formation and enhancement of exocytosis induced by A β ₁₋₄₂ oligomers in neuronal SH-SY5Y cells using MTT assay (data not shown) but it showed interesting neuroprotective effects against the late neuronal death elicited by A β ₁₋₄₂ oligomers.

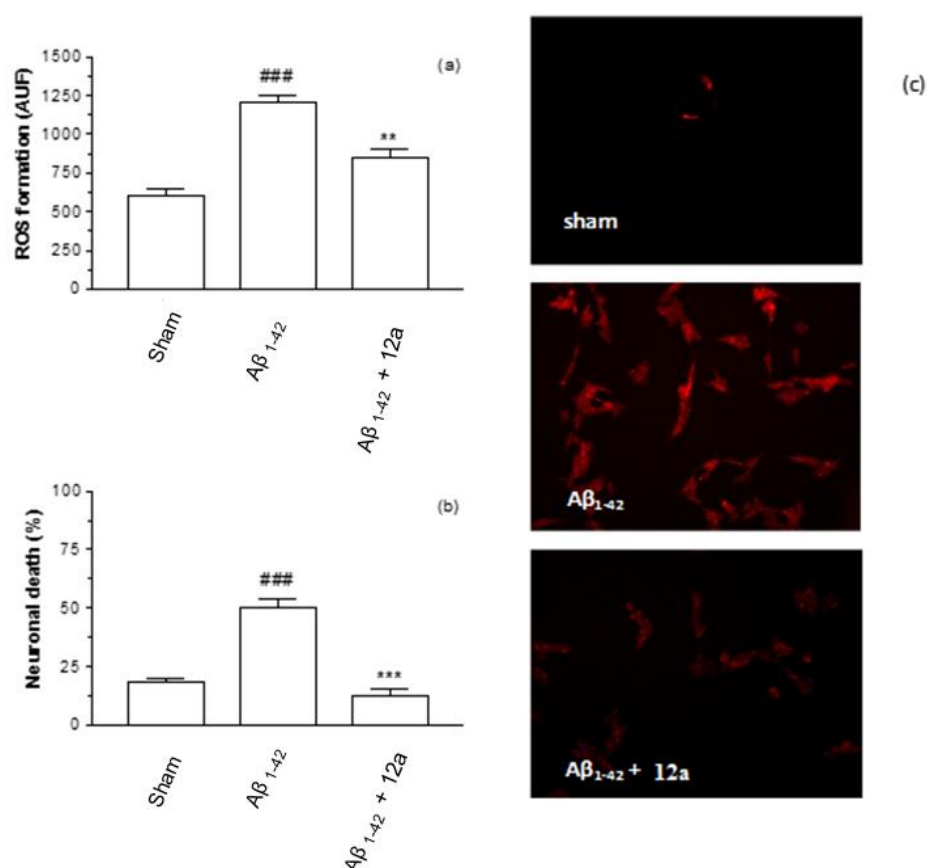


Fig. 12. Compound **12a** counteracts ROS formation and neuronal death induced by A β ₁₋₄₂ oligomers in neuronal SH-SY5Y cells. The cells were treated with 20 μ M of compound **12a** and A β ₁₋₄₂ oligomers (20 μ M) for either 4 h (a) or 24 h (b). At the end of the treatment, intracellular ROS formation and neuronal death were determined using DCFDA and propidium iodide probe (as described in the experimental section). (c) Representative images of ROS formation. The results are expressed as a percentage of control cells. The values are reported as mean \pm SD of three independent experiments (^{###}p<0.001 vs sham; ^{**}p<0.01, ^{***}p<0.001 vs treated with A β ₁₋₄₂ oligomers).

2.8. *In vivo* COX-1, COX-2 and 5-LOX activity evaluation

A recent study suggested that the pharmacophoric subunit derived from curcumin could display anti-inflammatory effects through the inhibition of cyclooxygenases 1 (COX-1) and 2 (COX-2), and 5-lipoxygenase (5-LOX) [35]. In this context, we evaluated the ability of compounds **12a** and **12c** to inhibit the activity of COX-1, COX-2 and 5-LOX of mice treated with the compounds and carrageenan, a pro-inflammatory lipopolysaccharide. In particular, COX-1, COX-2 and 5-LOX activities were measured in mice serum by using enzyme-linked immunosorbent assay. As shown in **Fig. 13**, compounds **12a**, **12c** and indomethacin, a positive control, significantly decreased the activity of COX-1 (inhibition of 40%, 30% and 50%, respectively) and COX-2 (27%, 60% and 42%, respectively); by contrast, only compound **12a** was able to inhibit 5-LOX activity (30%). Face to these results, compound **12a** showed the widest inhibitory activity profile on COX-1, COX-2 and 5-LOX.

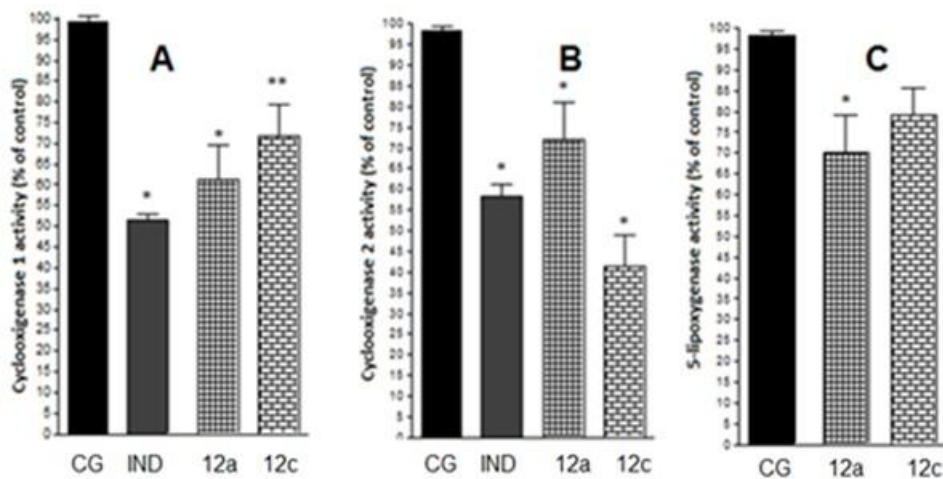


Fig. 13. Effect of compounds **12a** and **12c** on COX-1, COX-2 and 5-LOX activity in mice treated with carrageenan (CG). Mice were treated with compounds **12a**, **12c** (100 μ mol/kg, p.o) and indomethacin (IND, 100 μ mol/kg, p.o.) 1 h before intraplantar injection of carrageenan (400 μ g/paw). After 3 h, the COX-1, COX-2 and 5-LOX activity was determined as reported in the Experimental section. Values are expressed as mean \pm SEM (n=8) in terms of enzymatic activity percentage (*P<0.05 compared to the carrageenan group; **P<0.01 compared to the carrageenan group and the indomethacin group).

2.9. *In vivo* anti-inflammatory activity evaluation

It is currently accepted that inflammation is a hallmark of AD pathogenesis. Therefore, suppression of the neuroinflammation process may be a potential therapeutic approach against AD [36], [37], [38]. Thus, compounds **12a-c** were additionally evaluated for their *in vivo* anti-inflammatory effects. These compounds were firstly assayed in the formalin-induced antinociceptive model at a dose of 100 $\mu\text{mol/kg}$ p.o. The formalin test consists of two distinct phases. In the first one (neurogenic phase), a peripheral nociceptive effect due to formalin activation of tissue nociceptors is observed. In a second phase (inflammatory phase), the nociceptive effect is observed as a consequence of the release of several pro-inflammatory molecules (e.g. histamine, serotonin and bradykinin) in an acute inflammatory response [39], [40]. According to our results depicted in **Fig. 14**, only compounds **12a** and **12c** exhibited a significant antinociceptive activity in comparison to the control and indomethacin. Compound **12a** showed an antinociceptive response in both first and second phases, while compound **12c** was significantly active only in the inflammatory phase. In agreement with these results, compounds **12a** and **12c** were capable of reducing the time of licking during the inflammatory phase, suggesting that both have an anti-inflammatory effect, which could be a result of inhibition of formation and/or liberation of inflammatory mediators or by directly blocking their receptors [41]. In addition, compounds **12a** and **12c** did not alter motor performance in the open field model, confirming that the reduced licking time observed in the formalin test was not due to motor impairment (data not shown).

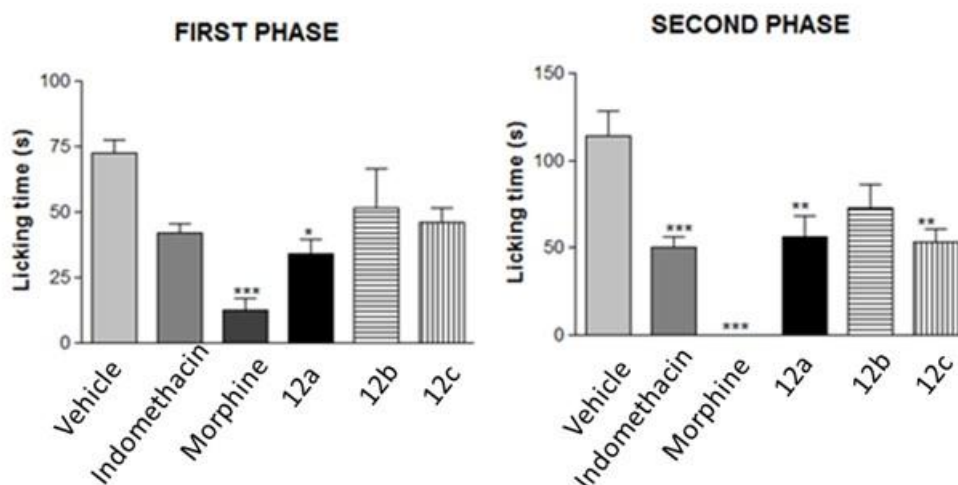


Fig. 14. Effect of compounds **12a**, **12b** and **12c** in a mice model of formalin-induced inflammatory pain. Mice were pre-treated orally with vehicle, compounds **12a-c** (100 $\mu\text{mol/kg}$), indomethacin (100 $\mu\text{mol/kg}$), morphine (39 $\mu\text{mol/kg}$) or vehicle (saline + DMSO 2%) prior to formalin administration. The total time spent licking the hindpaw was measured in the first and second phases after intraplantar injection of formalin. Values are expressed as mean \pm SEM (n=8) (* $p<0.05$, ** $p<0.01$, and *** $p<0.001$ compared to control group).

Taking into account the effects of compounds **12a** and **12c** in the second phase of the formalin test, they were then selected for further anti-inflammatory evaluation in LPS-induced peritonitis, carrageenan-induced paw edema and Von Frey models. Leukocyte migration to the inflammation site is a fundamental event in the onset of the inflammatory response [42]. Considering that this cell migration inhibition is also one of the characteristic effects of anti-inflammatory drugs, compounds **12a** and **12c** were evaluated in the LPS-induced peritonitis assay. This acute model of inflammation is used to evaluate leukocyte migration by the count of total leukocytes released during acute inflammation response after intraperitoneal administration of a phlogistic agent [43]. Results depicted in **Fig. 15** show that both compounds **12a** and **12c** significantly inhibited leukocyte migration in comparison to the control group (vehicle + LPS) and dexamethasone, reinforcing their anti-inflammatory properties.

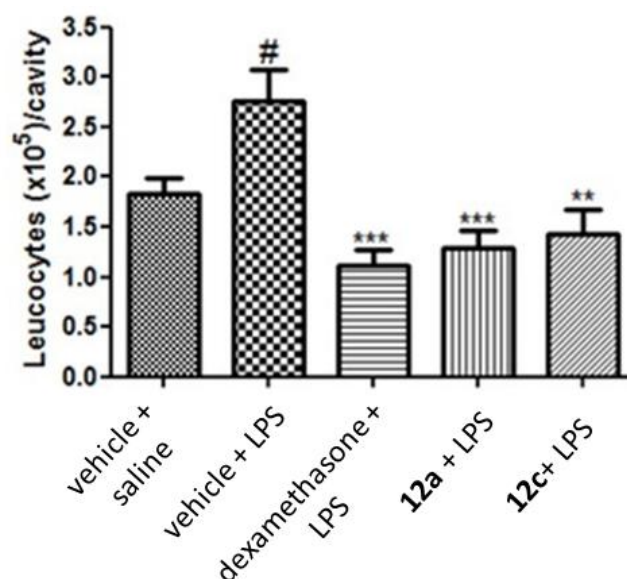


Fig. 15. Effect of compounds **12a** and **12c** in a mouse model of LPS-induced peritonitis. Mice were pre-treated orally with compounds **12a** and **12c** (100 μ mol/kg), dexamethasone (10 mg/kg, p.o.) or vehicle (saline + DMSO 2%) prior to LPS administration. The number of leukocytes recruited in the peritoneal cavity was determined. Values are expressed as mean \pm SEM (n=8). #P<0.05 compared with the saline + vehicle group; ***P<0.01, **P<0.01 and *P<0.05 compared with the vehicle + LPS group.

In another approach, compounds **12a** and **12c** were additionally tested for their ability to interfere in the carrageenan-induced mechanical hypernociception (Von Frey test). In this model, it is evaluated the animal sensitivity to a mechanical stimulus after induced-hyperalgesia by an intraplantar injection of carrageenan. The induction of hypernociception by carrageenan occurs through activation of the cytokine cascade that leads to the release of inflammatory mediators (e.g. prostaglandins), which cause the activation of A δ and C fiber sensory nerve endings, increasing the local flow and vascular permeability by the release of substance P and neurokinin A [44], [45]. The results shown in **Fig. 16 A** and **B** demonstrate that administration of carrageenan caused hyperalgesia with the peak of effect in the 3rd hour after intraplantar administration. Compounds **12a** and **12c** exhibited a significant antinociceptive effect after the 3rd hour of treatment. Compound **12a** showed a very similar effect to indomethacin used as drug control, while **12c** was shown to be active during all periods of the experiment with a greater breadth of statistical significance compared to the indomethacin and vehicle groups. As depicted in **Fig. 16 B**, both compounds exhibited their maximum anti-

inflammatory activity in the 3rd hour after treatment, with a fast decrease in their effectiveness after this time.

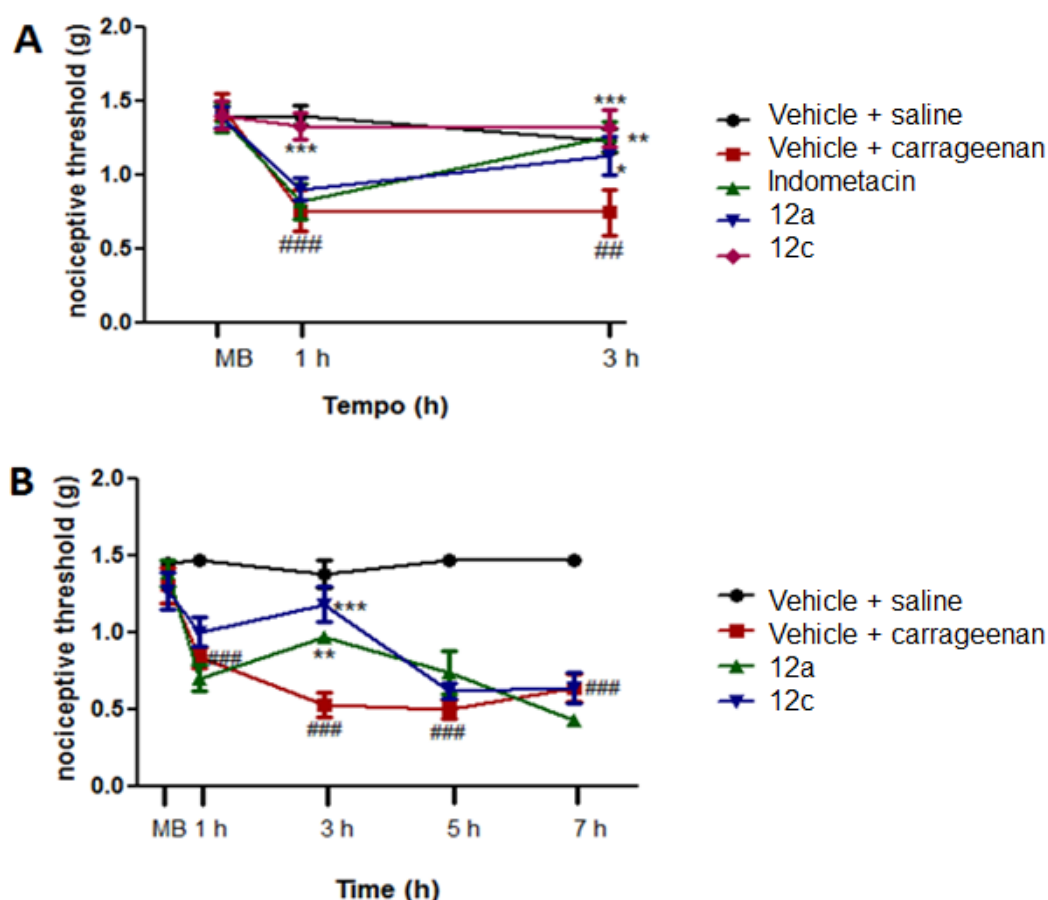


Fig. 16. Effect of compounds **12a** and **12c** on mechanical hyperalgesia in a mice model of carrageenan-induced paw edema. Mice were pre-treated orally with compounds **12a** and **12c** (100 μ mol/kg p.o) or indomethacin (100 μ mol/kg p.o) prior to intraplantar injection of carrageenan (100 μ g/paw). The results are presented as threshold for touch sensitivity (weight in grams). Values are expressed as mean \pm SEM (n=8). ### P<0.01 compared with the saline + vehicle group; *** P<0.01, **P<0.01 and *P<0.05 compared with the vehicle + carrageenan group.

Aiming to confirm the anti-inflammatory effect of compounds **12a** and **12c**, we also performed the carrageenan-induced paw edema assay. In this model, the development of edema induced by carrageenan is a biphasic event. The early phase (1–2 h) is mainly mediated by histamine, serotonin and bradykinin, followed by a late phase (3–6 h) sustained by the release of prostaglandins and NO produced by an inducible isoform of cyclooxygenase (COX-2) and NO-synthase (iNOS) [46], [47]. In this assay, compounds **12a** and **12c** promoted a significant decrease in the formation of

carrageenan-induced paw edema in comparison to the vehicle group (**Fig. 17**). The inhibitory profile of both compounds was similar to indomethacin, showing a maximum effect at the 3rd hour, with a higher potency for compound **12a**. The mechanism of action of indomethacin is produced by blockade of cyclooxygenases and, in turn, preventing the biosynthesis of prostaglandins. Taking all these results together, it is possible to suggest that compounds **12a** and **12c** exert their anti-inflammatory effect by this same mechanism of action.

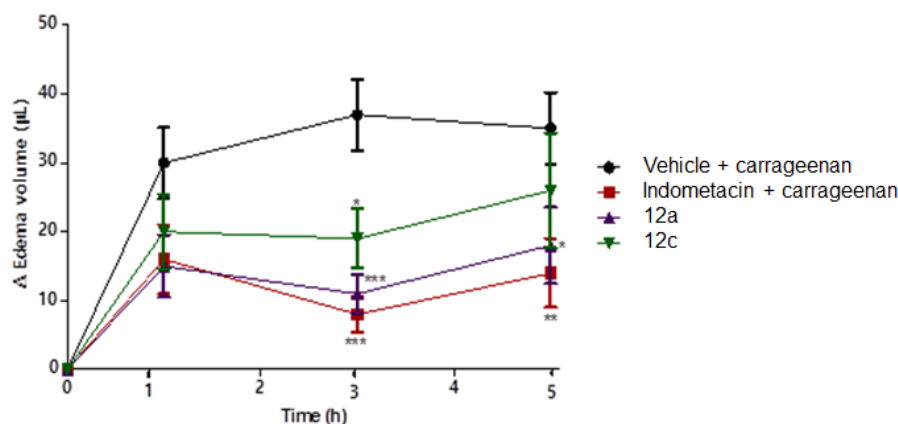


Fig. 17. Effect of compounds **12a** and **12c** in a mouse model of carrageenan-induced paw edema. Mice were pre-treated orally with compounds **12a** and **12c** (100 $\mu\text{mol/kg}$ p.o) or indomethacin (100 $\mu\text{mol/kg}$ p.o) prior to intraplantar injection of carrageenan (Cg, 100 $\mu\text{g/paw}$). The results are presented as the paw volume (μL) variation in relation to the basal values. Values are expressed as mean \pm SEM (n=8). *P<0.05, **P<0.01, ***P<0.001 compared with control group.

3. EXPERIMENTAL SECTION

3.1. Chemistry

All chemicals used were purchased from Sigma Aldrich. Solvents were purified and dried by standard procedures. Reactions were monitored by thin layer chromatography (TLC) on aluminum plates precoated with silica gel 60 F254 and the spots were visualized using a UV lamp ($\lambda = 254$ nm). Chromatographic separations were performed on silica gel (90-150 μm ; Merck) columns by flash chromatography. NMR spectra of target compounds were measured on a Bruker AC-300 spectrometer operating at 300 MHz for ^1H and 75 MHz for ^{13}C MHz and IR spectra were performed on Thermo Scientific Nicolet iS50 FT-IR spectrometer.

3.1.1. General procedures for the preparation of compounds **9a-9g**

A mixture of 4-piperidine methanol (1.2 mmol) and functionalized benzaldehydes (1.0 mmol) in 10 mL of anhydrous methanol and molecular sieve 4A° was stirred for 1 h. The solution of sodium cyanoborohydride (1.0 mmol) and zinc chloride (0.5 mmol) in anhydrous methanol (10 mL) also was stirred for 1 hour in r.t. After two hours the solutions were mixed and stirring was continued for 72 hours. The reaction mixture was treated with 0.1 M NaOH (10 mL) and extracted with ethyl acetate. The combined extracts were washed with brine, dried, and evaporated to dryness. Purification of the crude products were purified by flash column chromatography using DCM-MeOH (8:2) as eluents to afford **9a-9g**.

3.1.1.1. 1-benzyl piperidine-4-methanol (**9a**)

IR-ATR (cm^{-1}) 3340, 3084, 3026, 2915, 1600, 1494, 1451, 1256, 1040, 736, 697. NMR ^1H (δ , CDCl_3 , 300 MHz): 7.23-7.31 (m, 4H, HAr), 3.50 (s, 2H, CH_2Ar), 3.45 (d, 2H, $J=6.3$ Hz, CH_2OH), 2.87-2.94 (m, 2H, $\text{CH}_2\text{CH}_2\text{N}$), 1.96 (t, $J=11.7$ Hz, 2H, $\text{CH}_2\text{CH}_2\text{N}$), 1.66-1.72 (m, 2H, $\text{CH}_2\text{CH}_2\text{N}$), 1.21-1.34 (m, 2H, $\text{CH}_2\text{CH}_2\text{N}$), 1.42-1.55 (m, 1H, CH_2CHCH_2). NMR ^{13}C (δ , CDCl_3 , 75 MHz): 137.74, 129.41, 128.13, 127.04, 67.34, 63.39, 53.34, 38.35, 28.59.

3.1.1.2. 1-(4-nitrobenzyl) piperidine-4-methanol (**9b**)

IR-ATR (cm^{-1}) 3306, 3103, 2945, 1604, 1595, 1511, 1443, 1347, 1252, 1036, 849, 803. NMR ^1H (δ , CDCl_3 , 300 MHz): 8.17 (d, 2H, $J=9.0$ Hz, HAr), 7.51 (d, 2H, $J=8.2$ Hz, HAr), 3.58 (s, 2H, CH_2Ar), 3.51 (d, 2H, $J=6.3$ Hz, CH_2OH), 2.85-2.88 (m, 2H, $\text{CH}_2\text{CH}_2\text{N}$), 1.98-2.07 (m, 2H, $\text{CH}_2\text{CH}_2\text{N}$), 1.71-1.74 (m, 2H, $\text{CH}_2\text{CH}_2\text{N}$), 1.27-1.37 (m, 2H, $\text{CH}_2\text{CH}_2\text{N}$), 1.45-1.60 (m, 1H, CH_2CHCH_2). NMR ^{13}C (δ , CDCl_3 , 75 MHz): 147.08, 129.46, 123.47, 129.46, 146.79, 147.08, 67.82, 62.54, 53.60, 38.39, 28.78.

3.1.1.3. 1-(4-methoxybenzyl) piperidine-4-methanol (**9c**)

IR-ATR (cm^{-1}) 3361, 3072, 2926, 1611, 1583, 1511, 1244, 1178, 1034, 851, 818. NMR ^1H (δ , CDCl_3 , 300 MHz): 6.84 (d, 2H, $J=8.7$ Hz, HAr), 7.22 (d, 2H, $J=8.7$ Hz, HAr), 3.44 (s, 2H, CH_2Ar), 3.45 (d, 2H, $J=6.4$, CH_2OH), 3.79 (OCH_3), 2.86-2.92 (m, 2H, $\text{CH}_2\text{CH}_2\text{N}$), 1.93 (t, $J=11.7$, 2H, $\text{CH}_2\text{CH}_2\text{N}$), 1.66-1.72 (m, 2H, $\text{CH}_2\text{CH}_2\text{N}$), 1.20-1.33 (m, 2H, $\text{CH}_2\text{CH}_2\text{N}$), 1.41-1.53 (m, 1H, CH_2CHCH_2). NMR ^{13}C (δ , CDCl_3 , 75 MHz): 159.24, 131.32, 126.91, 113.78, 66.60, 61.60, 52.51, 37.67, 27.60.

3.1.1.4. 1-(4-chlorobenzyl) piperidine-4-methanol (**9d**)

IR-ATR (cm^{-1}) 3326, 3056, 2919, 1596, 1576, 1489, 1253, 1039, 843, 802. NMR ^1H (δ , CDCl_3 , 300 MHz): 7.20-7.29 (m, 4H, HAr), 3.42 (s, 2H, CH_2Ar), 3.39 (d, 2H, $J=6.3$ Hz, CH_2OH), 2.80-2.85 (m, 2H, $\text{CH}_2\text{CH}_2\text{N}$), 1.87-1.95 (m, 2H, $\text{CH}_2\text{CH}_2\text{N}$), 1.62-1.68 (m, 2H, $\text{CH}_2\text{CH}_2\text{N}$), 1.16-1.29 (m, 2H, $\text{CH}_2\text{CH}_2\text{N}$), 1.36-1.45 (m, 1H, CH_2CHCH_2). NMR ^{13}C (δ , CDCl_3 , 75 MHz): 136.30, 130.65, 132.70, 128.24, 67.18, 62.53, 53.24, 38.23, 28.52.

3.1.1.5. 1-(4-bromobenzyl) piperidine-4-methanol (**9e**)

IR-ATR (cm^{-1}) 3343, 3054, 2941, 1639, 1592, 1490, 1239, 1039, 1072, 844, 803. NMR ^1H (δ , CDCl_3 , 300 MHz): 7.43 (d, 2H, $J=8.5$ Hz, HAr), 7.20 (d, 2H, $J=8.5$ Hz, HAr), 3.45 (s, 2H, CH_2Ar), 3.47 (d, 2H, $J=6.4$ Hz, CH_2OH), 2.85-2.92 (m, 2H, $\text{CH}_2\text{CH}_2\text{N}$), 1.92-2.00 (m, 2H, $\text{CH}_2\text{CH}_2\text{N}$), 1.68-1.73 (m, 2H, $\text{CH}_2\text{CH}_2\text{N}$), 1.21-1.36 (m, 2H, $\text{CH}_2\text{CH}_2\text{N}$), 1.42-1.56 (m, 1H, CH_2CHCH_2). NMR ^{13}C (δ , CDCl_3 , 75 MHz): 137.27, 130.89, 131.27, 120.82, 67.76, 62.60, 53.34, 38.44, 28.59.

3.1.1.6. 1-(4-morpholinobenzyl) piperidine-4-methanol (**9f**)

IR-ATR (cm^{-1}) 3374, 3034, 1611, 1515, 1449, 1217, 1068, 1114, 924. NMR ^1H (δ , CDCl_3 , 300 MHz): 7.22 (d, 2H, $J=8.4$ Hz, HAr), 6.86 (d, 2H, $J=8.7$ Hz, HAr), 3.86 (t, $J=9.6$ Hz, 2H, $\text{NCH}_2\text{CH}_2\text{O}$), 3.44 (s, 2H, CH_2Ar), 3.48 (d, 2H, $J=6.3$ Hz, CH_2OH), 3.15 (t, $J=9.6$ Hz, 2H, $\text{NCH}_2\text{CH}_2\text{O}$), 2.88-2.94 (m, 2H, $\text{CH}_2\text{CH}_2\text{N}$), 1.90-2.00 (m, 2H, $\text{CH}_2\text{CH}_2\text{N}$), 1.67-1.73 (m, 2H, $\text{CH}_2\text{CH}_2\text{N}$), 1.22-1.35 (m, 2H, $\text{CH}_2\text{CH}_2\text{N}$), 1.43-1.53 (m, 1H, CH_2CHCH_2). NMR de ^{13}C (δ , CDCl_3 , 75 MHz): 131.30, 124.59, 115.23, 151.01, 66.48, 66.77, 61.19, 52.15, 48.90, 37.49, 27.20.

3.1.1.7. 1-(1,3dioxolbenzyl-5-ylmethyl)-piperidine-4-methanol (**9g**)

IR-ATR (cm^{-1}) 3369, 3068, 2943, 1502, 1491, 1441, 1209, 1243, 1100, 1033, 872, 808. NMR ^1H (δ , CDCl_3 , 300 MHz): 6.86 (s, 1H, HAr), 6.74 (s, 2H, HAr), 5.93 (s, 2H, OCH_2O), 3.43 (s, 2H, CH_2Ar), 3.48 (d, 2H, $J=7.2$ Hz, CH_2OH), 2.88-2.94 (m, 2H, $\text{CH}_2\text{CH}_2\text{N}$), 1.92-2.01 (m, 2H, $\text{CH}_2\text{CH}_2\text{N}$), 1.68-1.73 (m, 2H, $\text{CH}_2\text{CH}_2\text{N}$), 1.23-1.36 (m, 2H, $\text{CH}_2\text{CH}_2\text{N}$), 1.43-1.55 (m, 1H, CH_2CHCH_2). NMR ^{13}C (δ , CDCl_3 , 75 MHz): 131.72, 147.59, 146.64, 122.49, 109.73, 107.85, 100.89, 67.73, 63.03, 53.19, 38.45, 28.59.

3.1.2. General procedures for the preparation of compounds **12a-12n**

To a mixture of ferulic acid or iso-ferulic acid (1 mmol) in dry dichloromethane (5mL), thionyl chloride (10 mmol) and DMF (25 μL) were added, and the resulting solution was stirred under argon atmosphere for 60 min at rt. After evaporation of the solvent, the residue was dissolved in dry dichloromethane (10 mL) and slowly added to the appropriate intermediate (**9a-g**) (1.5 mmol). The reaction mixture was stirred for 15 min at r.t. under argon atmosphere. The solvent was evaporated under vacuum. Purification of the crude products was by flash column chromatography using DCM-MeOH (9.5:0.5) as eluents to afford **12a-12n**.

3.1.2.1. (*E*)-(1-benzylpiperidin-4-yl)methyl 3-(4-hydroxy-3-methoxyphenyl)acrylate (**12a**)

IR-ATR (cm^{-1}): 3422, 3062, 2937, 1703, 1631, 1588, 1451, 1281, 1029, 1154, 736, 698. NMR ^1H (δ , CDCl_3 , 300 MHz): 6.88 (d, 1H, $J=8.1$, HAr), 7.01 (d, 1H, $J=1.8$, HAr),

7.04 (dd, 1H, $J=8.2$ and 1.9 , HAr), 7.30-7.31 (m, 5H, HAr), 7.60 (d, 1H, $J=15.9$, $\text{CH}=\text{CH}$), 6.27 (d, 1H, $J=15.9$, $\text{CH}=\text{CH}$), 4.06 (d, 2H, $J=6.0$, COOCH_2), 2.93-2.97 (m, 2H, $\text{CH}_2\text{CH}_2\text{N}$), 1.97-2.05 (m, 2H, $\text{CH}_2\text{CH}_2\text{N}$), 1.71-1.76 (m, 3H, $\text{CH}_2\text{CH}_2\text{N}$ and CH_2CHCH_2), 1.40-1.49 (m, 2H, $\text{CH}_2\text{CH}_2\text{N}$), 3.53 (s, 2H, CH_2Ar), 3.89 (s, 3H, OCH_3). NMR ^{13}C (δ , CDCl_3 , 75 MHz): 114.95, 146.98, 148.19, 109.44, 126.83, 123.04, 144.88, 115.31, 167.35, 68.65, 35.38, 28.74, 53.18, 63.32, 137.80, 129.38, 127.12, 128.21, 55.87. HRMS (ESI) calculated for $\text{C}_{23}\text{H}_{27}\text{NO}_4$ $[\text{M}+\text{H}]^+$: m/z 382.20183; found: 382.20205

3.1.2.2. (*E*)-(1-(4-nitrobenzyl)piperidin-4-yl)methyl 3-(4-hydroxy-3-methoxyphenyl)acrylate (**12b**)

IR-ATR (cm^{-1}): 3373, 3072, 2992, 1698, 1631, 1588, 1509, 1343, 1256, 1149, 1028, 844, 741. NMR ^1H (δ , CDCl_3 , 300 MHz): 6.87 (d, 1H, $J=8.0$, HAr), 7.00 (d, 1H, $J=1.8$, HAr), 7.09 (dd, 1H, $J=8.1$ and 1.8 , HAr), 7.48 (d, 2H, $J=8.7$, HAr), 8.13 (d, 2H, $J=8.7$, HAr), 7.58 (d, 1H, $J=15.9$, $\text{CH}=\text{CH}$), 6.26 (d, 1H, $J=15.9$, $\text{CH}=\text{CH}$), 4.05 (d, 2H, $J=6.0$, COOCH_2), 2.84-2.87 (m, 2H, $\text{CH}_2\text{CH}_2\text{N}$), 1.98-2.06 (m, 2H, $\text{CH}_2\text{CH}_2\text{N}$), 1.70-1.75 (m, 3H, $\text{CH}_2\text{CH}_2\text{N}$ and CH_2CHCH_2), 1.31-1.45 (m, 2H, m, 2H, $\text{CH}_2\text{CH}_2\text{N}$), 3.56 (s, 2H, CH_2Ar), 3.87 (s, 3H, OCH_3). NMR ^{13}C (δ , CDCl_3 , 75 MHz): 115.05, 146.62, 148.27, 109.57, 126.94, 123.15, 145.06, 115.35, 167.44, 68.69, 35.41, 28.98, 53.50, 62.58, 147.19, 123.56, 129.64, 147.07, 56.01. HRMS (ESI) calculated for $\text{C}_{23}\text{H}_{26}\text{N}_2\text{O}_6$ $[\text{M}+\text{H}]^+$: m/z 427.18691; found: 427.18635

3.1.2.3. (*E*)-(1-(4-bromobenzyl)piperidin-4-yl)methyl 3-(4-hydroxy-3-methoxyphenyl)acrylate (**12c**)

IR-ATR (cm^{-1}): 3428, 3063, 2937, 1699, 1630, 1588, 1509, 1253, 1115, 1030, 726. NMR ^1H (δ , CDCl_3 , 300 MHz): 6.85 (d, 1H, $J=7.5$, HAr), 7.05 (d, 1H, $J=2.0$, HAr), 7.09 (dd, 1H, $J=8.3$ and 2.0 , HAr), 7.19 (d, 2H, $J=8.4$, HAr), 7.42 (d, 2H, $J=8.3$, HAr), 7.62 (d, 1H, $J=15.9$, $\text{CH}=\text{CH}$), 6.31 (d, 1H, $J=15.9$, $\text{CH}=\text{CH}$), 4.05 (d, 2H, $J=6.0$, COOCH_2), 2.86-2.90 (m, 2H, $\text{CH}_2\text{CH}_2\text{N}$), 1.93-2.01 (m, 2H, $\text{CH}_2\text{CH}_2\text{N}$), 1.60-1.76 (m, 3H, $\text{CH}_2\text{CH}_2\text{N}$ and CH_2CHCH_2), 1.31-1.47 (m, 2H, $\text{CH}_2\text{CH}_2\text{N}$), 3.44 (s, 2H, CH_2Ar), 3.90 (s, 3H, OCH_3). NMR ^{13}C (δ , CDCl_3 , 75 MHz): 113.02, 149.15, 151.06, 109.54, 127.32, 122.58, 144.60, 115.70, 167.15, 69.91, 35.37, 28.88, 53.14, 62.51, 136.72, 130.73,

131.21, 120.69, 55.83. HRMS (ESI) calculated for $C_{23}H_{26}BrNO_4$ $[M+H]^+$: m/z 460.11234; found: 460.11243

3.1.2.4. (*E*)-(1-(4-morpholinobenzyl)piperidin-4-yl)methyl 3-(4-hydroxy-3-methoxyphenyl)acrylate (**12d**)

IR-ATR (cm^{-1}): 3427, 3067, 2954, 1698, 1609, 1439, 1378, 1261, 1159, 1118, 923, 805. NMR de 1H (δ , $CDCl_3$, 300 MHz): 6.93 (d, 1H, $J=7.5$, HAr), 7.09-7.17 (m, 4H, HAr), 6.88 (d, 2H, $J=8.3$, HAr), 7.56 (d, 1H, $J=15.9$, $CH=CH$), 6.35 (d, 1H, $J=15.9$, $CH=CH$), 4.00 (d, 2H, $J=6.5$, $COOCH_2$), 2.90-2.95 (m, 2H, CH_2CH_2N), 1.93-2.02 (m, 2H, CH_2CH_2N), 1.63-1.68 (m, 3H, CH_2CH_2N and CH_2CHCH_2), 1.34-1.46 (m, 2H, CH_2CH_2N), 3.46 (s, 2H, CH_2Ar), 3.80 (s, 3H, OCH_3), 3.16 (t, 4H, $J=4.6$, CH_2NCH_2), 3.74 (t, 4H, CH_2OCH_2). NMR ^{13}C (δ , $CDCl_3$, 75 MHz): 115.48, 147.27, 148.54, 109.71, 127.90, 123.16, 145.12, 115.71, 167.44, 68.55, 35.34, 28.43, 52.83, 62.42, 130.80, 129.28, 115.22, 150.74, 56.01, 49.42, 67.02. HRMS (ESI) calculated for $C_{27}H_{34}N_2O_5$ $[M+H]^+$: m/z 467.25459; found: 467.25468

3.1.2.5. (*E*)-(1-(4-methoxybenzyl)piperidin-4-yl)methyl 3-(4-hydroxy-3-methoxyphenyl)acrylate (**12e**)

IR-ATR (cm^{-1}): 3383, 3067, 2935, 1713, 1631, 1583, 1244, 1157, 1117, 1029, 973, 814. NMR 1H (δ , $CDCl_3$, 300 MHz): 6.98 (d, 1H, $J=7.5$, HAr), 7.06 (d, 1H, $J=2.00$, HAr), 7.10 (dd, 1H, $J=7.5$ and 2.0 , HAr), 7.30 (d, 2H, $J=7.2$, HAr), 6.83 (d, 2H, $J=7.2$, HAr), 7.59 (d, 1H, $J=15.1$, $CH=CH$), 6.42 (d, 1H, $J=15.1$, $CH=CH$), 4.05 (d, 2H, $J=6.8$, $COOCH_2$), 2.96-2.99 (m, 2H, CH_2CH_2N), 2.00-2.08 (m, 2H, CH_2CH_2N), 1.73-1.78 (m, 3H, CH_2CH_2N and CH_2CHCH_2), 1.39-1.51 (m, 2H, CH_2CH_2N), 3.56 (s, 2H, CH_2Ar), 3.92 (s, 3H, OCH_3), 3.80 (s, 3H, CH_3). NMR ^{13}C (δ , $CDCl_3$, 75 MHz): 114.83, 146.88, 148.09, 109.38, 126.85, 123.05, 144.84, 115.37, 167.30, 68.63, 35.37, 28.64, 52.88, 62.50, 126.89, 130.63, 113.58, 158.80, 55.25, 55.92. HRMS (ESI) calculated for $C_{24}H_{29}NO_5$ $[M+H]^+$: m/z 412.21239; found: 412.2134

3.1.2.6. (*E*)-(1-benzylpiperidin-4-yl)methyl 3-(3-hydroxy-4-methoxyphenyl)acrylate (**12f**)

IR-ATR (cm⁻¹): 3371, 3060, 2935, 1698, 1629, 1588, 1510, 1450, 1249, 1029, 1154, 740, 698. NMR ¹H (δ, CDCl₃, 300 MHz): 6.97 (d, 1H, *J*=7.5, HAr), 7.12 (m, 2H, HAr), 7.28-7.31 (m, 5H, HAr), 7.60 (d, 1H, *J*=15.1, CH=CH), 6.35 (d, 1H, *J*=15.1, CH=CH), 4.05 (d, 2H, *J*=6.7, COOCH₂), 2.94-2.98 (m, 2H, CH₂CH₂N), 1.98-2.06 (m, 2H, CH₂CH₂N), 1.73-1.77 (m, 3H, CH₂CH₂N and CH₂CHCH₂), 1.41-1.49 (m, 2H, CH₂CHCH₂) 3.54 (s, 2H, CH₂Ar), 3.83 (s, 3H, OCH₃). NMR ¹³C (δ, CDCl₃, 75 MHz): 110.78, 149.08, 145.36, 114.51, 125.67, 121.65, 144.43, 115.18, 167.26, 68.32, 35.03, 28.65, 52.28, 62.87, 137.50, 129.32, 127.52, 128.52, 55.87. HRMS (ESI) calculated for C₂₃H₂₇NO₄ [M+H]⁺: m/z 382.20183; found: 382.2032.

3.1.2.7. (*E*)-(1-(4-nitrobenzyl)piperidin-4-yl)methyl 3-(3-hydroxy-4-methoxyphenyl)acrylate (**12g**)

IR-ATR (cm⁻¹): 3319, 3062, 2938, 1698, 1630, 1590, 1516, 1346, 1243, 1118, 1028, 855, 729. NMR ¹H (δ, CDCl₃, 300 MHz): 6.96 (d, 1H, *J*=8.0, HAr), 7.09-7.11 (m, 2H, HAr), 7.49 (d, 2H, *J*=8.7, HAr), 8.18 (d, 2H, *J*=8.7, HAr), 7.59 (d, 1H, *J*=15.9, CH=CH), 6.35 (d, 1H, *J*=15.9, CH=CH), 4.05 (d, 2H, *J*=6.5, COOCH₂), 2.85-2.90 (m, 2H, CH₂CH₂N), 2.00-2.09 (m, 2H, CH₂CH₂N), 1.72-1.78 (m, 3H, CH₂CH₂N and CH₂CHCH₂), 1.34-1.47 (m, 2H, CH₂CH₂N), 3.55 (s, 2H, CH₂Ar), 3.85 (s, 3H, OCH₃). NMR ¹³C (δ, CDCl₃, 75 MHz): 110.75, 149.19, 145.34, 114.41, 125.61, 121.40, 144.23, 115.15, 167.69, 68.49, 35.49, 29.01, 53.55, 62.63, 147.05, 123.59, 129.68, 147.30, 56.09. HRMS (ESI) calculated for C₂₃H₂₆N₂O₆ [M+H]⁺: m/z 427.18691; found: 427.18705

3.1.2.8. (*E*)-(1-(4-bromobenzyl)piperidin-4-yl)methyl 3-(3-hydroxy-4-methoxyphenyl)acrylate (**12h**)

IR-ATR (cm⁻¹): 3406, 3063, 2934, 1698, 1630, 1589, 1510, 1253, 1116, 1029, 772.

NMR

¹H (δ, CDCl₃, 300 MHz): 6.98 (d, 1H, *J*=7.5, HAr), 7.09 (d, 1H, *J*=2.0, HAr), 7.13 (dd, 1H, *J*=7.4 and 2.0, HAr), 7.20 (d, 2H, *J*=8.4, HAr), 7.43 (d, 2H, *J*=7.5, HAr), 7.60 (d, 1H, *J*=15.1, CH=CH), 6.41 (d, 1H, *J*=15.1, CH=CH), 4.05 (d, 2H, *J*=6.7, COOCH₂), 1.69-1.76 (m, 3H, CH₂CH₂N and CH₂CHCH₂), 1.34-1.46 (m, 2H, CH₂CH₂N), 2.87-2.93

(m, 2H, CH₂CH₂N), 1.94-2.03 (m, 2H, CH₂CH₂N), 3.45 (s, 2H, CH₂Ar), 3.88 (s, 3H, OCH₃). NMR ¹³C (δ, CDCl₃, 75 MHz): 111.23, 148.45, 145.01, 114.17, 125.22, 121.63, 144.21, 115.37, 167.39, 69.84, 35.24, 28.92, 52.98, 62.43, 136.89, 130.34, 131.12, 120.42, 55.92. HRMS (ESI) calculated for C₂₃H₂₆BrNO₄ [M+H]⁺: m/z 460.11234; found: 460.11370

3.1.2.9. (*E*)-(1-(4-morpholinobenzyl)piperidin-4-yl)methyl 3-(3-hydroxy-4-methoxyphenyl)acrylate (**12i**)

IR- ATR (cm⁻¹): 3395, 3066, 2948, 1711, 1631, 1589, 1464, 1268, 1155, 1119, 979, 815. NMR de ¹H (δ, CDCl₃, 300 MHz): 7.00 (d, 1H, *J*=7.5, HAr), 7.07-7.12 (m, 2H, HAr), 7.20 (d, 2H, *J*=7.6, HAr), 6.81 (d, 2H, *J*=8.3, HAr), 7.58 (d, 1H, *J*=15.1, CH=CH), 6.32 (d, 1H, *J*=15.1, CH=CH), 4.03 (d, 2H, *J*=6.5, COOCH₂), 1.70-1.73 (m, 3H, CH₂CH₂N and CH₂CHCH₂), 1.34-1.46 (m, 2H, CH₂CH₂N), 2.91-2.95 (m, 2H, CH₂CH₂N), 1.94-2.03 (m, 2H, CH₂CH₂N), 3.45 (s, 2H, CH₂Ar), 3.83 (s, 3H, OCH₃), 3.16 (t, 4H, *J*=4.6, CH₂NCH₂), 3.74 (t, 4H, *J*=4.7, CH₂OCH₂). NMR ¹³C (δ, CDCl₃, 75 MHz): 110.91, 148.12, 146.48, 114.81, 125.95, 121.26, 144.98, 115.20, 167.36, 68.75, 35.68, 28.34, 52.63, 62.12, 130.83, 128.74, 115.89, 150.68, 56.05, 49.42, 66.89. HRMS (ESI) calculated for C₂₇H₃₄N₂O₅ [M+H]⁺: m/z 467.25459; found: 467.25471

3.1.2.10. (*E*)-(1-(4-methoxybenzyl)piperidin-4-yl)methyl 3-(3-hydroxy-4-methoxyphenyl)acrylate (**12j**)

IR-ATR (cm⁻¹): 3400, 3063, 2932, 1698, 1629, 1585, 1509, 1365, 1243, 1154, 1119, 1028, 974, 813. NMR ¹H (δ, CDCl₃, 300 MHz): 7.00 (d, 1H, *J*=7.5, HAr), 7.11 (d, 1H, *J*=2.1, HAr), 7.06 (dd, 1H, *J*= 7.5 and 2.0, HAr), 7.31 (d, 2H, *J*=7.5, HAr), 6.95 (d, 2H, *J*=7.5, HAr), 7.59 (d, 1H, *J*=15.1, CH=CH), 6.45 (d, 1H, *J*=15.1, CH=CH), 4.07 (d, 2H, *J*=6.5, COOCH₂), 2.93-2.97 (m, 2H, CH₂CH₂N), 1.97-2.06 (m, 2H, CH₂CH₂N), 1.70-1.76 (m, 3H, CH₂CH₂N and CH₂CHCH₂), 1.38-1.50 (m, 2H, CH₂CH₂N), 3.56 (s, 2H, CH₂Ar), 3.87 (s, 3H, OCH₃), 3.78 (s, 3H, CH₃). NMR ¹³C (δ, CDCl₃, 75 MHz): 111.03, 148.07, 146.98, 114.38, 125.72, 121.75, 144.74, 115.07, 167.42, 68.23, 35.43, 28.32, 52.41, 62.31, 127.09, 130.89, 113.61, 158.70, 55.50, 55.94. HRMS (ESI) calculated for C₂₄H₂₉NO₅ [M+H]⁺: m/z 412.21239; found: 412.21244

3.1.2.11. (*E*)-(1-(4-chlorobenzyl)piperidin-4-yl)methyl 3-(4-hydroxy-3-methoxyphenyl)acrylate (**12k**)

IR-ATR (cm⁻¹): 3386, 3064, 2935, 1704, 1632, 1588, 1509, 1248, 1116, 1029, 807. NMR de ¹H (δ, CDCl₃, 300 MHz): 6.89 (d, 1H, *J*=8.2, HAr), 7.06 (d, 1H, *J*=2.1, HAr), 7.10 (dd, 1H, *J*= 7.5 and 2.2, HAr), 7.59 (d, 1H, *J*=15.9, CH=CH), 6.41 (d, 1H, *J*=15.9, CH=CH), 4.07 (d, 2H, *J*=6.4, COOCH₂), 2.87-2.91 (m, 2H, CH₂CH₂N), 1.94-2.03 (m, 2H, CH₂CH₂N), 1.70-1.75 (m, 3H, CH₂CH₂N and CH₂CHCH₂), 1.37-1.46 (m, 2H, CH₂CH₂N), 3.55 (s, 2H, CH₂Ar), 7.24-7.26 (d, 2H, *J*=7.3, HAr), 3.84 (s, 3H, OCH₃). NMR ¹³C (δ, CDCl₃, 75 MHz): 114.88, 147.35, 148.66, 109.76, 126.47, 122.96, 145.05, 115.28, 167.35, 68.38, 35.12, 28.34, 52.89, 62.15, 135.54, 130.84, 128.34, 133.01, 55.79. HRMS (ESI) calculated for C₂₃H₂₆ClNO₄ [M+H]⁺: m/z 416.16286; found: 416.16289.

3.1.2.12. (*E*)-(1-(benzo[d][1,3]dioxol-5-ylmethyl)piperidin-4-yl)methyl 3-(4-hydroxy-3-methoxyphenyl)acrylate (**12l**)

IR-ATR (cm⁻¹): 3388, 3069, 2923, 1701, 1630, 1588, 1503, 1368, 1240, 1117, 1032, 927, 808. NMR ¹H (δ, CDCl₃, 300 MHz): 6.99 (d, 1H, *J*=7.2, HAr), 7.06 (d, 1H, *J*=1.8, HAr), 7.10 (dd, 1H, *J*= 8.4 and 1.9, HAr), 7.57 (d, 1H, *J*=15.1, CH=CH), 6.42 (d, 1H, *J*=15.0, CH=CH), 4.04 (d, 2H, *J*=6.0, COOCH₂), 2.93-2.95 (m, 2H, CH₂CH₂N), 1.93-2.00 (m, 1H, CH₂CH₂N), 1.63-1.67 (m, 3H, CH₂CH₂N and CH₂CHCH₂), 1.39-1.45 (m, 2H, CH₂CH₂N), 3.53 (s, 2H, CH₂Ar), 6.85 (s, 1H, HAr), 6.78 (m, HAr), 3.84 (s, 3H, OCH₃), 5.95 (s, 2H, OCH₂O). NMR ¹³C (δ, CDCl₃, 75 MHz): 115.00, 147.68, 148.26, 109.68, 126.94, 123.15, 144.91, 115.66, 166.76, 69.53, 34.00, 29.60, 52.96, 62.72, 131.39, 107.92, 147.04, 146.75, 109.50, 122.43, 55.95, 100.95. HRMS (ESI) calculated for C₂₄H₂₇NO₆ [M+H]⁺: m/z 426.19166; found: 426.1917

3.1.2.13. (*E*)-(1-(4-chlorobenzyl)piperidin-4-yl)methyl 3-(3-hydroxy-4-methoxyphenyl)acrylate (**12m**)

IR-ATR (cm⁻¹): 3393, 3062, 2936, 1712, 1631, 1585, 1509, 1261, 1115, 1030, 806. NMR ¹H (δ, CDCl₃, 300 MHz): 6.93 (d, 1H, *J*=8.2, HAr), 7.09-7.12 (m, 2H, HAr), 7.59

(d, 1H, $J=15.9$, $\text{CH}=\text{CH}$), 6.43 (d, 1H, $J=15.9$, $\text{CH}=\text{CH}$), 4.05 (d, 2H, $J=6.5$, COOCH_2), 2.85-2.93 (m, 2H, $\text{CH}_2\text{CH}_2\text{N}$), 1.93-2.02 (m, 2H, $\text{CH}_2\text{CH}_2\text{N}$), 1.69-1.76 (m, 3H, $\text{CH}_2\text{CH}_2\text{N}$ and CH_2CHCH_2), 1.36-1.44 (m, 2H, $\text{CH}_2\text{CH}_2\text{N}$), 3.56 (s, 2H, CH_2Ar), 7.23-7.26 (d, 2H, $J=7.3$, HAr), 3.82 (s, 3H, OCH_3). NMR ^{13}C (δ , CDCl_3 , 75 MHz): 110.78, 145.36, 148.66, 114.28, 126.47, 122.96, 144.23, 115.19, 167.36, 68.39, 35.12, 28.34, 52.89, 62.15, 135.55, 130.84, 128.52, 133.02, 55.80. HRMS (ESI) calculated for $\text{C}_{23}\text{H}_{26}\text{ClNO}_4$ $[\text{M}+\text{H}]^+$: m/z 416.16286; found: 416.16292

3.1.2.14. (*E*)-(1-(benzo[d][1,3]dioxol-5-ylmethyl)piperidin-4-yl)methyl 3-(3-hydroxy-4-methoxyphenyl)acrylate (**12n**)

IR-ATR (cm^{-1}): 3374, 3125, 2926, 1703, 1631, 1588, 1506, 1369, 1256, 1119, 1030, 905, 727. NMR ^1H (δ , CDCl_3 , 300 MHz): 7.00 (d, 1H, $J=7.5$, HAr), 7.09 (d, 1H, $J=1.8$, HAr), 7.14 (dd, 1H, $J=8.4$ and 1.9 , HAr), 7.59 (d, 1H, $J=15.1$, $\text{CH}=\text{CH}$), 6.42 (d, 1H, $J=15.0$, $\text{CH}=\text{CH}$), 4.05 (d, 2H, $J=6.5$, COOCH_2), 2.90-2.97 (m, 2H, $\text{CH}_2\text{CH}_2\text{N}$), 1.99-2.04 (m, 2H, $\text{CH}_2\text{CH}_2\text{N}$), 1.70-1.74 (m, 3H, $\text{CH}_2\text{CH}_2\text{N}$ and CH_2CHCH_2), 1.37-1.48 (m, 2H, $\text{CH}_2\text{CH}_2\text{N}$), 3.55 (s, 2H, CH_2Ar), 6.85 (s, 1H, HAr), 6.80 (m, HAr), 3.80 (s, 3H, OCH_3), 5.97 (s, 2H, OCH_2O). NMR ^{13}C (δ , CDCl_3 , 75 MHz): 111.45, 149.38, 145.44, 114.12, 125.12, 121.14, 144.23, 115.38, 167.32, 69.01, 35.76, 28.35, 51.39, 62.98, 132.19, 107.43, 146.19, 147.04, 108.96, 121.92, 55.95, 100.83. HRMS (ESI) calculated for $\text{C}_{24}\text{H}_{27}\text{NO}_6$ $[\text{M}+\text{H}]^+$: m/z 426.19166; found: 426.19049

3.2. Anti-cholinesterase activity assays

For the *in vitro* evaluation of inhibition of EeAChE (E.C. 3.1.1.7, type V-S, purified from *Electrophorus electricus*) and eqBuChE (E.C. 3.1.1.8, purified from equine serum), kinetic assays were performed by Ellman's method [48] modified for 96-well plates as previously described [49,50]. In a well containing 20 μL of enzyme (0.5 U/mL) and 5 μL of 5,5'-dithiobis-(2-nitrobenzoic) acid (10 mM) in sodium phosphate buffer (0.1 M, pH 7.4), 100 μL of compound solution (two times

concentrated) were added along with 55 μL of phosphate buffer (0.1M, pH 7.4) to achieve 180 μL . 10 min later, 20 μL of the appropriate substrate (acetylthiocholine or butyrylthiocholine iodide, 0.5 M final) were added and absorbance was read in a SpectraMax 250 spectrophotometer (Molecular Devices) at 412 nm during 5 min with 12 s intervals. Progression curves were acquired through SOFTmax PRO 5.0 (Molecular Devices) from which maximum hydrolysis velocity was estimated and analysis performed with Prism (Graphpad). The substrate competition data from two experiments were pooled and analyzed by global fitting of alternate inhibition models, selected by likelihood criteria [49]. All reagents were purchased from Sigma-Aldrich (Brazil). Derivatives were dissolved at 0.05 M in DMSO and diluted in phosphate buffer to the described concentrations immediately before use. The solvent had no detectable effect at the highest final concentration used (0.2% v.v.).

3.3. Molecular docking study with AChE

In this work we evaluated the possible binding modes of three compounds **12a**, **12b** and **12c** in three different states of AChE: the free and acetylated enzyme as well as the Michaelis complex (AChE complexed with the substrate ACh). All models were based on the structure of the AChE complexed with the potent inhibitor donepezil at resolution of 2.35Å (PDB code 4ey7) [51]. Since the three-dimensional structure of the acetylated enzyme has not been experimentally determined yet, we generated the acetylated model from the X-ray structure of AChE-donepezil (PDB code 4ey7), since this inhibitor is proposed to inhibit the enzyme on both free and acetylated forms [52]. The presence of conserved waters in the binding site was analyzed through superimposition of diverse AChE-inhibitor complexes, *i.e.* 4ey7 [51], 1q83, 1q84 [53] and 2ckm [54]. The four water molecules W729, W722, W731, W737 and W931 were extracted from the structure of the AChE complexed with donepezil (PDB code 4ey7) and considered explicitly during the docking experiments. The AChE structures were prepared using the Protein Preparation Wizard [55] tool in Maestro Suite 2014 (version 9.7, Schrödinger, LLC, New York, NY, 2014). In this preparatory step, all hydrogen atoms were added, the protonation states and tautomers of His residues were optimized using PROPKA at pH 7.0 [56]. The energy grid was generated in the Glide module (Glide, version 6.2, Schrödinger, LLC, New York, NY, 2014) and the coordinate center was based on the native ligand present in the 4ey7 complex (X: 9.6, Y: -6.7 and Z: -

35.73). The structures of the compounds were manually designed in the Maestro Suite 2014 (version 9.7, Schrödinger, LLC, New York, NY, 2014), while the structure of the reference ligand donepezil was extracted from the AChE-donepezil complex (PDB code 4ey7). Only the E diastereomers of the compounds were considered for docking studies. All structures were prepared with LigPrep (version 2.9, Schrödinger, LLC, New York, NY, 2014) and the protonation states were determined with Epik in pH = 7.0±0.5 [57,58]. Docking studies were performed with the Glide software (version 6.2, Schrödinger, LLC, New York, NY, 2014) using the Extra Precision Docking mode [59] and all other options were maintained with default values. Only the top ranked pose for each configuration of each compound (according to the XP Pose Rank) and the ring conformation with the lowest potential energy were maintained for the analyses. The docking score reported is the score provided by the scoring function utilized by the Extra Precision Docking mode.

3.4. DPPH scavenging activity

The ability of compounds **12a–12n** to scavenge DPPH free radicals was evaluated according to the method of Hatano and cols. [60]. A concentration series (100, 50, 25 and 12.5 µM in ethanol) of each compound was prepared. A 4mL aliquot of sample solution was mixed with 1 mL of DPPH (0.5 mM in ethanol). This mixture was vigorously shaken at room temperature for 30 min. The absorbance of the mixture was then measured at 517 nm. A low absorbance value indicates effective free radical scavenging. Each solution was analysed in triplicate, and the average values were plotted to obtain the EC₅₀ against DPPH by linear regression. The activity of trolox, a recognized antioxidant, ferulic acid and *iso*-ferulic acid was used as a standard over the same range of concentrations. The radical-scavenging activity was evaluated as the percentage of inhibition according to the following equation: %inhibition = [(absorbance of control – absorbance of sample)/absorbance of control)] × 100.

3.5. Metal chelation assay

The chelating studies were performed in ethanol using UV–vis spectrophotometer (SHIMADZU UV-1800) with wavelength ranging from 200 to 400

nm. The absorption spectra of **12a**, **12b** and **12c** (75 μ M) alone or in the presence of CuCl₂, FeSO₄, FeCl₃ or ZnCl₂ (150 μ M) in ethanol were recorded at room temperature.

3.6. Evaluation of *in vitro* neurotoxicity, anti-oxidant and neuroprotective activity

3.6.1. Cell Cultures

Human neuronal (SH-SY5Y) cells were routinely grown in Dulbecco's modified Eagle' Medium (DMEM) supplemented with 10% fetal bovine serum, 2 mmol/L-glutamine, 50 U/mL penicillin and 50 μ g/mL streptomycin at 37 °C in a humidified incubator with 5% CO₂.

3.6.2. Determination of neurotoxicity induced by compounds

Neuronal viability in terms of mitochondrial activity was evaluated with the 3-(4,5-dimethyl-2-thiazolyl)-2,5-diphenyl-2H-tetrazolium bromide (MTT) assay, as previously described [61]. Briefly, SH-SY5Y cells were seeded in 96-well plates at 2×10^4 cells/well, incubated for 24 h and subsequently treated with various concentrations of compounds (1.25–40 μ M) for 24 h at 37 °C in 5% CO₂. The treatment medium was then replaced with MTT (5 mg/mL) in phosphate-buffered saline (PBS) for 2 h at 37 °C in 5% CO₂. After washing with PBS, the formazan crystals were dissolved with isopropanol. The amount of formazan was measured (570 nm, reference filter 690 nm) using a multilabel plate reader (VICTOR™ X3, PerkinElmer, Waltham, MA, USA). The neurotoxicity is expressed as concentration of compound resulting in 50% inhibition of cell viability.

3.6.3. Determination of intracellular ROS formation induced by H₂O₂ and metals

ROS formation was determined using the fluorescent probe 2',7'-dichlorodihydrofluorescein diacetate (DCFH-DA), as previously reported with minor modification [61]. Briefly, SH-SY5Y cells were seeded in 96-well plates at 3×10^4 cells/well and incubated for 24 h at 37 °C in 5% CO₂. Subsequently cell culture medium was removed and 100 μ L of DCFH-DA (10 μ g/mL) were added to each wells. After 30 min of incubation at room temperature the DCFH-DA solution was replaced with

various concentrations of compounds (5-40 μM) and either H_2O_2 (100 μM) or $\text{FeSO}_4/\text{H}_2\text{O}_2$, or $\text{CuSO}_4/\text{H}_2\text{O}_2$ (100 $\mu\text{M}/25 \mu\text{M}$). In parallel, the SH-SY5Y cells were also treated with compounds for 24 h before the treatment with H_2O_2 . The ROS formation was measured (excitation at 485 nm and emission at 535 nm) using a multilabel plate reader (VICTOR™ X3). The values are expressed as arbitrary fluorescence units (AUF).

3.6.4. Determination of intracellular glutathione levels

Cellular GSH levels were determined by the monochlorobimane (MCB) assay in 96-well plates as previously reported with minor modification [62]. Briefly, SH-SY5Y cells were seeded in 96-well plates at 2×10^4 cells/well, incubated for 24 h and subsequently treated with 20 μM of compound for various treatment times (3-24 h) at 37 °C in 5% CO_2 . The treatment medium was then replaced with MCB (50 μM) in PBS for 30 min at 37 °C in 5% CO_2 . The amount of GSH was measured (excitation at 360 nm and emission at 465 nm) using a multilabel plate reader (VICTOR™ X3, PerkinElmer, Waltham, MA, USA). The values are expressed as a percentage of control cells.

3.6.5. Nuclear extraction and Nrf2 binding activity assay

Nuclear extraction and Nrf2 binding activity assay were performed using the Nuclear Extract and TransAM Nrf2 kits (Active Motif, Carlsbad, CA, USA), respectively, according to the manufacturer's guidelines. Protein concentration in samples was measured using the Bio-Rad Protein Assay Dye reagent. Briefly, SH-SY5Y cells were seeded in cultures dishes (size 60 mm) at 2×10^6 cells/dish, incubated for 24 h and subsequently treated with 20 μM of compound for various treatment times (1-6 h) at 37 °C in 5% CO_2 . At the end of treatment, 20 μg of nuclear extract was evaluated by TransAM Nrf2 Kit. The values are expressed as a percentage of control cells.

3.6.6. $\text{A}\beta_{1-42}$ oligomer preparation

A β ₁₋₄₂ peptides (Bachem AG, Bubendorf, Switzerland) were first dissolved in hexafluoroisopropanol to 1 mg/mL, sonicated, incubated at room temperature for 24 h and lyophilized. The resulting unaggregated A β ₁₋₄₂ film was dissolved with dimethylsulfoxide and stored at 20°C until use. The A β ₁₋₄₂ aggregation to oligomeric form was prepared as previously described [63]. The morphology of oligomeric A β ₁₋₄₂ forms obtained was checked using transmission electron microscopy.

3.6.7. Determination of intracellular ROS formation induced by A β ₁₋₄₂ oligomers

ROS formation induced by A β ₁₋₄₂ oligomers was determined using the dihydroethidium (DHE), as previously reported [64]. Briefly, SH-SY5Y cells were cultured in BD Falcon™ 8-well Culture slides (surface area 0.7 cm²/well) at 1x10⁴ cells/well for 24 h. The cells were then treated for 3 h with compound (20 μ M) and A β ₁₋₄₂ oligomers (10 μ M) at 37 °C in 5% CO₂. At the end of treatment, the cells were washed and incubated with DHE (10 μ M) for 30 min in the dark. After removal of the probes, cells were washed with PBS and incubated with DMEM serum free for 1 h at 37°C. Intracellular ROS formation was measured under a fluorescence microscope (Eclipse Ti Inverted microscope, Nikon instruments Europe, Amsterdam, Netherlands). Fluorescence images were captured with NIS-Elements imaging software (Nikon instruments Europe). Four randomly selected areas with 50–100 cells in each were analyzed and the values obtained are expressed as arbitrary fluorescence units (AUF).

3.6.8. Determination of MTT Formazan Exocytosis induced by A β ₁₋₄₂ oligomers

MTT Formazan Exocytosis induced by A β ₁₋₄₂ oligomers was determined using MTT assay, as previously reported [65]. Briefly, SH-SY5Y cells were seeded in 96-well plates at 3 x 10⁴ cells/well, incubated for 24 h and subsequently treated with compound (20 μ M) and A β ₁₋₄₂ oligomers (10 μ M) for 4 at 37 °C in 5% CO₂. The treatment medium was then replaced with MTT (5 mg/mL) in PBS for 2 h at 37 °C in 5% CO₂. The SH-SY5Y cells were then examined under a microscope and photographed to detect MTT formazan exocytosis. The needle-like crystals on the surface of the cells treated with only A β ₁₋₄₂ oligomers, which are easily visible under a light microscope, represent exocytosed MTT formazan.

3.6.9. Determination of neuronal death induced by A β ₁₋₄₂ oligomers

Neuronal death induced by A β ₁₋₄₂ oligomers was determined using the fluorescent probe propidium iodide (PI), as previously reported with minor modification [66]. Briefly, SH-SY5Y cells were seeded in 96-well plates 5x10³ cells/well, incubated for 24 h and subsequently treated with compound (20 μ M) and A β ₁₋₄₂ oligomers (10 μ M) for 24 at 37 °C in 5% CO₂. The treatment medium was then replaced with PI (25 μ g/mL) in PBS for 10 min at 37 °C. The stained cells with PI were then examined under a fluorescence microscope (Eclipse Ti Inverted microscope). Four randomly selected areas with 50–100 cells in each were analyzed and the values obtained are expressed as percentage of death cells and calculated by the formula: (propidium iodide-positive cells/n total cells) x 100.

3.7. Evaluation of anti-inflammatory activity *in vivo*

3.7.1. Animals

Adult male Swiss mice (22–28 g) were obtained from the Central Animal Facility of the Federal University of Alfenas and housed under controlled light (12:12 h light–dark cycle; lights on at 6:00 am) and temperature conditions (23 \pm 1°C) with access to water and food ad libitum. Except for the night before the experiments, when they were submitted to an overnight fast. The animals were allowed to habituate to the housing facilities for at least 1 week before the experiments began. The experimental protocol was approved by the local Research Ethics Committee of the Federal University of Alfenas (protocol n° 633/2015).

3.7.2. Formalin-induced nociception

This test was based on the method by Hunskaar et al. [67]. A formalin solution (5% in 0.9% saline) was injected (20 μ l/paw) into the sub-plantar region of the right hind paw, and the animals were individually placed in transparent observation chambers, as previously described [41],[68]. Oral treatments (p.o) with vehicle, indomethacin **12a**, **12b** and **12c** (100 μ mol/kg) were given 1 h prior to formalin injection (n=8 per group). Morphine (39 μ mol/kg) was administrated (i.p.) 30 min before the test.

Animals were observed from 0 to 5 min (neurogenic pain) and from 20 to 30 min (inflammatory pain) after the formalin injection, and the time spent licking the injected paw was recorded and considered as indicative of nociception.

3.7.3. Open field behavioral test

To discard the possible nonspecific muscle relaxant or sedative effects of **12a** and **12c**, the motor performance of the mice was evaluated in the open-field apparatus as previously reported by Veloso [68]. Groups of mice (n=8) were treated with vehicle or **12a** or **12b** 1 h before the test. Each animal was placed in the center of the open-field arena. Four squares of apparatus were defined as the center, and the 12 squares along the walls were considered the periphery. Each mouse (n = 8 per group) was placed in the exact center of the arena, and activity was scored as a line crossing when a mouse removed all four paws from one square and entered another. Line crossings among the central four squares and the peripheral 12 squares of the open field were counted separately.

3.7.4. Peritonitis induced by lipopolysaccharide

To assess the possible effect of the compounds **12a** and **12c** on leukocyte recruitment to the peritoneal cavity, the animals (n=8 per group) were orally pre-treated with vehicle, **12a** or **12c** (100 μ mol/kg), or dexamethasone (1 mg/kg), and 30 min later, lipopolysaccharide (LPS) from *Escherichia coli* serotype 026:B6 dissolved in sterile saline was administered at a dose of 100 μ g/kg (i.p). Four hours after the injection of LPS, mice were killed with an inhalatory overdose of halothane, and the cells from the peritoneal cavities were harvested by an injection of 10 ml of PBS containing 0.5% sodium citrate. The abdomens were gently massaged, and the blood-free cell suspension

was carefully aspirated with a syringe. Abdominal washings were placed into plastic tubes, and total cell counts were performed immediately in a Neubauer chamber. The results were presented as the number of cells per cavity [69].

3.7.5. Mechanical nociceptive paw test

The mechanical nociceptive thresholds of the animals was evaluated according to the up-and-down method [70] using the Von Frey filaments (North Coast Medical, Inc. Morgan Hill, CA). The mice were placed in acrylic boxes and on a wire screen, providing access to the paw of the animals 60 min before test. The Von Frey filaments were applied perpendicularly on the plantar region outside of the hind paw of animals, for a period of approximately 4 seconds or until the animal demonstrates nocifensive behavior, characterized by paw withdrawal, then licking and/or "flinching". The evaluation of mice begins with the 0.4 g filament. In this method, at least 6 tests, with 10 second intervals, were made per animal. The absence of animal's response to a particular filament led to use other filament of greater mass, until there is a withdrawal response. Vehicle, **12a** or **12c** or indomethacin was orally administered 1 h before the intraplantar injection of carrageenan (100 µg/paw). The results are expressed by the average nociceptive threshold in grams.

3.7.6. Carrageenan-induced mice paw edema.

Paw edema was measured with a plethysmometer (Ugo Basile, mod 7140) based on the method of Levy (1969) [71]. The basal volume of the right hind paw was determined before the administration of any drug and the animals were divided into experimental groups (n=10 per groups) in such a way that the mean volumes of the different groups were similar. The vehicle (DMSO 2%, sterile saline), **12a**, **12c**, indomethacin (100 µmol/kg) were orally administered 1 h before the intraplantar (i.pl.) injection of carrageenan (400 µg/20 µl). The paw volume was measured 1, 3 and 5 h after the injection of the inflammatory stimulus. The results are presented as the paw volume (µL) variation in relation to the basal values.

3.7.7. COX-1/2 and 5-LOX production

Mice were treated with drugs (100 $\mu\text{mol/kg}$, p.o.) or vehicle 1 h before carrageenan i.pl. injection. Three hours after carrageenan injection, the rats were anesthetized with chloral hydrate and blood samples were collected from the heart. Blood sample of different groups was centrifuged at 1500 rpm/20 min and the serum was collected and frozen at -70°C . The analysis of COX-1, COX-2 and 5-LOX protein expression was done according to the manufacturer's instruction (USCN Life Science Inc. for COX-1; R&D Systems for COX-2 and 5-LOX) using an antibody specific coated onto the wells. The plates are then read by a microplate reader at 450 nm [72,73]

3.7.8. Statistical analysis

The data obtained were analyzed using the GraphPad software program version 4.0 and expressed as mean \pm S.E.M. Statistical significances of differences among groups were evaluated by analysis of variance (ANOVA) followed by the Bonferroni test. p values less than 0.05 ($p < 0.05$) were considered significant.

4. CONCLUSIONS

In summary, a series of fourteen novel feruloyl-donepezil hybrids were designed and synthesized as multifunctional agents for the treatment of AD by fusing the pharmacophore of donepezil with a similar pattern with curcumin and ferulic acid.

Among all tested compounds, **12a**, **12b** and **12c** showed the highest inhibitory activities for EeAChE. Kinetic and molecular docking studies revealed that compounds **12a** and **12c** were a non-competitive inhibitors that could interact both with PAS of AChE. The selected compounds **12a-c** were further evaluated for various biological properties relevant for AD, including antioxidant activity (DPPH), neuroprotection against ROS and A β -induced toxicity, metal-chelating properties and anti-inflammatory effects *in vivo*. The results of the *in vitro* and *in vivo* assays demonstrated that compound **12a** shows multiple desirable effects, consistent with the intended MTDLs profile. This compound is the most potent inhibitor of AChE and also displays the

highest antioxidant activities in neuronal SH-SY5Y cells, both direct and indirect (activating the Keap1/Nrf2/ARE pathway), besides being a good biometal-chelator. Furthermore, our results suggest that compound **12a** has neuroprotective effects against the late neuronal death elicited by A β ₁₋₄₂ oligomers, and a significant *in vivo* anti-inflammatory activity in different models. Taking together, all these results suggest that **12a** could be considered as a potential multifunctional neuroprotective agent and a new lead candidate prototype for the treatment of AD.

Conflict of interest

The authors confirm that this article content has no conflicts of interest.

Acknowledgements

The authors are grateful to the Brazilian Agencies CAPES, FAPEMIG, CNPq and FINEP for financial support and fellowships.

References

- [1] F.P.D. Viegas, M.C.R. Simões, M.D. da Rocha, M.R. Castelli, M.S. Moreira, C. V. Junior, Alzheimer's Disease: Characterization, Evolution and Implications of the Neuroinflammatory Process, *Rev. Virtual Química*. 3 (2011). doi:10.5935/1984-6835.20110034.
- [2] A. Association, 2016 Alzheimer's Disease Facts and Figures, (2016). http://www.alz.org/documents_custom/2016-facts-and-figures.pdf.
- [3] M. Prince, A. Wimo, M. Guerchet, A. Gemma-Claire, Y.-T. Wu, M. Prina, World Alzheimer Report 2015: The Global Impact of Dementia - An analysis of prevalence, incidence, cost and trends, *Alzheimer's Dis. Int.* (2015) 84. doi:10.1111/j.0963-7214.2004.00293.x.
- [4] C. Haass, D.J. Selkoe, Soluble protein oligomers in neurodegeneration: lessons from the Alzheimer's amyloid beta-peptide., *Nat. Rev. Mol. Cell Biol.* 8 (2007) 101–112. doi:10.1038/nrm2101.

- [5] P.L. McGeer, E.G. McGeer, The amyloid cascade-inflammatory hypothesis of Alzheimer disease: Implications for therapy, *Acta Neuropathol.* 126 (2013) 479–497. doi:10.1007/s00401-013-1177-7.
- [6] V. Cavallucci, M. D’Amelio, F. Cecconi, A β Toxicity in Alzheimer’s Disease, *Mol. Neurobiol.* 45 (2012) 366–378. doi:10.1007/s12035-012-8251-3.
- [7] R. Bartus, R. Dean, B. Beer, A. Lippa, The cholinergic hypothesis of geriatric memory dysfunction, *Science.* 217 (1982) 408–414. doi:10.1126/science.7046051.
- [8] P. Anand, B. Singh, A review on cholinesterase inhibitors for Alzheimer’s disease, *Arch. Pharm. Res.* 36 (2013) 375–399. doi:10.1007/s12272-013-0036-3.
- [9] K. Jomova, D. Vondrakova, M. Lawson, M. Valko, Metals, oxidative stress and neurodegenerative disorders, *Mol. Cell. Biochem.* 345 (2010) 91–104. doi:10.1007/s11010-010-0563-x.
- [10] R. Gonzalez-Dominguez, T. Garcia-Barrera, J.L. Gomez-Ariza, Homeostasis of metals in the progression of Alzheimer’s disease, *BioMetals.* 27 (2014) 539–549. doi:10.1007/s10534-014-9728-5.
- [11] M.A. Greenough, J. Camakaris, A.I. Bush, Metal dyshomeostasis and oxidative stress in Alzheimer’s disease, *Neurochem. Int.* 62 (2013) 540–555. doi:10.1016/j.neuint.2012.08.014.
- [12] M.T. Heneka, M.J. Carson, J. El Khoury, G.E. Landreth, F. Brosseron, D.L. Feinstein, A.H. Jacobs, T. Wyss-Coray, J. Vitorica, R.M. Ransohoff, K. Herrup, S.A. Frautschy, B. Finsen, G.C. Brown, A. Verkhratsky, K. Yamanaka, J. Koistinaho, E. Latz, A. Halle, G.C. Petzold, T. Town, D. Morgan, M.L. Shinohara, V.H. Perry, C. Holmes, N.G. Bazan, D.J. Brooks, S. Hunot, B. Joseph, N. Deigendesch, O. Garaschuk, E. Boddeke, C.A. Dinarello, J.C. Breitner, G.M. Cole, D.T. Golenbock, M.P. Kummer, Neuroinflammation in Alzheimer’s disease, *Lancet Neurol.* 14 (2015) 388–405. doi:10.1016/S1474-4422(15)70016-5.
- [13] M. L. Bolognesi, Polypharmacology in a Single Drug: Multitarget Drugs, *Curr. Med. Chem.* 20 (2013) 1639–1645. doi:10.2174/0929867311320130004.
- [14] K.S.T. Dias, C.T. de Paula, M.M. Riquiel, S.T.L. do Lago, K.C.M. Costa, S.M. Vaz, R.P. Machado, L.M.S. de Lima, C. Viegas Jr., Recent Applications of the Multi-Target Directed Ligands Approach for the Treatment of Alzheimer’s Disease, *Rev. Virtual Química.* 7 (2015). doi:10.5935/1984-6835.20150027.

- [15] K. Simone, T. Dias, C. Viegas, Multi-Target Directed Drugs: A Modern Approach for Design of New Drugs for the treatment of Alzheimer's Disease, *Curr. Neuropharmacol.* 12 (2014) 239–255.
- [16] L. Ismaili, B. Refouvelet, M. Benchekroun, S. Brogi, M. Brindisi, S. Gemma, G. Campiani, S. Filipic, D. Agbaba, G. Esteban, M. Unzeta, K. Nikolic, S. Butini, J. Marco-Contelles, Multitarget compounds bearing tacrine- and donepezil-like structural and functional motifs for the potential treatment of Alzheimer's disease, *Prog. Neurobiol.* (2016) 1–31. doi:10.1016/j.pneurobio.2015.12.003.
- [17] Z. Luo, J. Sheng, Y. Sun, C. Lu, J. Yan, A. Liu, H. Bin Luo, L. Huang, X. Li, Synthesis and evaluation of multi-target-directed ligands against Alzheimer's disease based on the fusion of donepezil and ebselen, *J. Med. Chem.* 56 (2013) 9089–9099. doi:10.1021/jm401047q.
- [18] M. Benchekroun, L. Ismaili, M. Pudlo, V. Luzet, T. Gharbi, B. Refouvelet, J. Marco-Contelles, Donepezil–ferulic acid hybrids as anti-Alzheimer drugs, *Future Med. Chem.* 7 (2015) 15–21. doi:10.4155/fmc.14.148.
- [19] S.-S. Xie, J.-S. Lan, X. Wang, Z.-M. Wang, N. Jiang, F. Li, J.-J. Wu, J. Wang, L.-Y. Kong, Design, synthesis and biological evaluation of novel donepezil-coumarin hybrids as multi-target agents for the treatment of Alzheimer's disease., *Bioorg. Med. Chem.* 24 (2016) 1528–39. doi:10.1016/j.bmc.2016.02.023.
- [20] S.-Y. Chen, Y. Chen, Y.-P. Li, S.-H. Chen, J.-H. Tan, T.-M. Ou, L.-Q. Gu, Z.-S. Huang, Design, synthesis, and biological evaluation of curcumin analogues as multifunctional agents for the treatment of Alzheimer's disease, *Bioorg. Med. Chem.* 19 (2011) 5596–5604. doi:10.1016/j.bmc.2011.07.033.
- [21] L. Fang, S. Gou, X. Liu, F. Cao, L. Cheng, Design, synthesis and anti-Alzheimer properties of dimethylaminomethyl- substituted curcumin derivatives, *Bioorg. Med. Chem. Lett.* 24 (2014) 40–43. doi:10.1016/j.bmcl.2013.12.011.
- [22] G. Gerenu, K. Liu, J.E. Chojnacki, J.M. Saathoff, P. Martínez-Martín, G. Perry, X. Zhu, H.G. Lee, S. Zhang, Curcumin/Melatonin Hybrid 5-(4-Hydroxy-phenyl)-3-oxo-pentanoic Acid [2-(5-Methoxy-1H-indol-3-yl)-ethyl]-amide Ameliorates AD-Like Pathology in the APP/PS1 Mouse Model, *ACS Chem. Neurosci.* 6 (2015) 1393–1399. doi:10.1021/acschemneuro.5b00082.
- [23] Y. Li, P. Peng, L. Tang, Y. Hu, Y. Hu, R. Sheng, Design, synthesis and evaluation of rivastigmine and curcumin hybrids as site-activated multitarget-directed ligands for Alzheimer's disease therapy, *Bioorg. Med. Chem.* 22 (2014)

4717–4725. doi:10.1016/j.bmc.2014.07.009.

- [24] P. Zhai, C.-L. Xia, J.-H. Tan, D. Li, T.-M. Ou, S.-L. Huang, L.-Q. Gu, Z.-S. Huang, Syntheses And Evaluation Of Asymmetric Curcumin Analogues As Potential Multifunctional Agents For The Treatment Of Alzheimer's Disease., *Curr. Alzheimer Res.* 12 (2015) 403–14. <http://www.ncbi.nlm.nih.gov/pubmed/25938868>.
- [25] G.K. Jayaprakasha, L. Jaganmohan Rao, K.K. Sakariah, Antioxidant activities of curcumin, demethoxycurcumin and bisdemethoxycurcumin, *Food Chem.* 98 (2006) 720–724. doi:10.1016/j.foodchem.2005.06.037.
- [26] Y. Tizabi, L.L. Hurley, Z. Qualls, L. Akinfiresoye, Relevance of the anti-inflammatory properties of curcumin in neurodegenerative diseases and depression, *Molecules.* 19 (2014) 20864–80879. doi:10.3390/molecules191220864.
- [27] K. Ono, K. Hasegawa, H. Naiki, M. Yamada, Curcumin Has Potent Anti-Amyloidogenic Effects for Alzheimer's β -Amyloid Fibrils *In Vitro*, *J. Neurosci. Res.* 75 (2004) 742–750. doi:10.1002/jnr.20025.
- [28] L. Shen, H.Y. Zhang, H.F. Ji, A theoretical study on Cu(II)-chelating properties of curcumin and its implications for curcumin as a multipotent agent to combat Alzheimer's disease, *J. Mol. Struct. Theochem.* 757 (2005) 199–202. doi:10.1016/j.theochem.2005.05.016.
- [29] A.A. Farooqui, Effects of Curcumin on Neuroinflammation in Animal Models and in Patients with Alzheimer Disease, in: *Ther. Potentials Curcumin Alzheimer Dis.*, Springer International Publishing Switzerland, (2016) 259–296. doi:10.1007/978-3-319-15889-1.
- [30] P.K. Kamat, A. Kalani, S. Rai, S. Swarnkar, S. Tota, C. Nath, N. Tyagi, Mechanism of Oxidative Stress and Synapse Dysfunction in the Pathogenesis of Alzheimer's Disease: Understanding the Therapeutics Strategies, *Mol. Neurobiol.* 53 (2016) 648–661. doi:10.1007/s12035-014-9053-6.
- [31] Y. Cai, Mei Sun, Jie Xing, Q. Luo, H. Corke, Structure–radical scavenging activity relationships of phenolic compounds from traditional Chinese medicinal plants, *Life Sci.* 78 (2006) 2872–2888. doi:10.1016/j.lfs.2005.11.004.
- [32] K.J. Barnham, A.I. Bush, Metals in Alzheimer's and Parkinson's Diseases, *Curr. Opin. Chem. Biol.* 12 (2008) 222–228. doi:10.1016/j.cbpa.2008.02.019.
- [33] A.T. Dinkova-Kostova, P. Talalay, Direct and indirect antioxidant properties of

- inducers of cytoprotective proteins, *Mol. Nutr. Food Res.* 52 (2008) 128–138. doi:10.1002/mnfr.200700195.
- [34] A. Rauk, Why is the amyloid beta peptide of Alzheimer's disease neurotoxic?, *Dalton Trans.* (2008) 1273–1282. doi:10.1039/b718601k.
- [35] V.R. Chinthalapally, REGULATION OF COX AND LOX BY CURCUMIN, in: B.A. Bharat, J.S. Young, S. Shishir (Eds.), *Mol. Targets Ther. Uses Curcumin Heal. Dis.*, Springer, New York, 2015: pp. 213–226.
- [36] F.L. Heppner, R.M. Ransohoff, B. Becher, Immune attack: the role of inflammation in Alzheimer disease, *Nat Rev Neurosci.* 16 (2015) 358–372. doi:10.1038/nrn3880.
- [37] M.T. Heneka, M.J. Carson, J. El Khoury, G.E. Landreth, F. Brosseron, D.L. Feinstein, A.H. Jacobs, T. Wyss-coray, J. Vitorica, R.M. Ransohoff, K. Herrup, S.A. Frautschy, B. Finsen, G.C. Brown, A. Verkhratsky, K. Yamanaka, J. Koistinaho, E. Latz, A. Halle, G.C. Petzold, T. Town, D. Morgan, M.L. Shinohara, V.H. Perry, C. Holmes, N.G. Bazan, D.J. Brooks, S. Hunot, B. Joseph, N. Deigendesch, O. Garaschuk, E. Boddeke, C.A. Dinarello, J.C. Breitner, G.M. Cole, D.T. Golenbock, M.P. Kummer, Neuroinflammation in Alzheimer's disease, *Lancet Neurol.* 14 (2015) 388–405. doi:10.1016/S1474-4422(15)70016-5.
- [38] C. Holmes, Review: Systemic inflammation and Alzheimer's disease, *Neuropathol. Appl. Neurobiol.* 39 (2013) 51–68. doi:10.1111/j.1365-2990.2012.01307.x.
- [39] C.R. Mcnamara, J. Mandel-brehm, D.M. Bautista, J. Siemens, K.L. Deranian, M. Zhao, N.J. Hayward, J.A. Chong, D. Julius, M.M. Moran, C.M. Fanger, TRPA1 mediates formalin-induced pain., *Proc. Natl. Acad. Sci. U. S. A.* 104 (2007) 30. doi:10.1073/pnas.0705924104.
- [40] C.V. Clarice, G.R. Vanessa, de O.A. Adolfo, da C.O. Cristina, F.G. Lindisley, P.D. Lucienir, D.D. Igor, K. Andre, de C.P. Andrea, Antinociceptive effects of *Maytenus imbricata* Mart. ex. Reissek (Celastraceae) root extract and its tingenone constituent, *J. Med. Plants Res.* 8 (2014) 68–76. doi:10.5897/JMPR2013.5085.
- [41] A.R.S. Santos, J.B. Calixto, Further evidence for the involvement of tachykinin receptor subtypes in formalin, and capsaicin models of pain in mice, *Neuropeptides.* 31 (1997) 381–389. doi:10.1016/S0143-4179(97)90075-5.

- [42] J.G. Geng, Directional migration of leukocytes: their pathological roles in inflammation and strategies for development of anti-inflammatory therapies., *Cell Res.* 11 (2001) 85–8. doi:10.1038/sj.cr.7290071.
- [43] E. García-Ramallo, T. Marques, N. Prats, J. Beleta, S.L. Kunkel, N. Godessart, Resident cell chemokine expression serves as the major mechanism for leukocyte recruitment during local inflammation., *J. Immunol.* 169 (2002) 6467–6473. doi:10.4049/jimmunol.169.11.6467.
- [44] L. Orlandi, F.C. Vilela, F. V. Santa-Cecília, D.F. Dias, G. Alves-Da-Silva, A. Giusti-Paiva, Anti-inflammatory and antinociceptive effects of the stem bark of *Byrsonima intermedia* A. Juss., *J. Ethnopharmacol.* 137 (2011) 1469–1476. doi:10.1016/j.jep.2011.08.032.
- [45] T.M. Cunha, W.A. Verri, J.S. Silva, S. Poole, F.Q. Cunha, S.H. Ferreira, A cascade of cytokines mediates mechanical inflammatory hypernociception in mice, *Proc. Natl. Acad. Sci.* 102 (2005) 1755–1760. doi:10.1073/pnas.0409225102.
- [46] F. V. Santa-Cecília, L.A.S. Freitas, F.C. Vilela, C.D.C. Veloso, C.Q. Da Rocha, M.E.C. Moreira, D.F. Dias, A. Giusti-Paiva, M.H. Dos Santos, Antinociceptive and anti-inflammatory properties of 7-epiclusianone, a prenylated benzophenone from *Garcinia brasiliensis*, *Eur. J. Pharmacol.* 670 (2011) 280–285. doi:10.1016/j.ejphar.2011.08.032.
- [47] K. Seibert, Y. Zhang, K. Leahy, S. Hauser, J. Masferrer, W. Perkins, L. Lee, P. Isakson, Pharmacological and biochemical demonstration of the role of cyclooxygenase 2 in inflammation and pain., *Proc. Natl. Acad. Sci. U. S. A.* 91 (1994) 12013–7. doi:10.1073/pnas.91.25.12013.
- [48] G.L. Ellman, K.D. Courtney, V. Andres, R.M. Featherstone, A new and rapid colorimetric determination of acetylcholinesterase activity, *Biochem. Pharmacol.* 7 (1961) 88–95. doi:10.1016/0006-2952(61)90145-9.
- [49] N.G. Castro, R.S. Costa, L.S.B. Pimentel, A. Danuello, N.C. Romeiro, C. Viegas, E.J. Barreiro, C.A.M. Fraga, V.S. Bolzani, M.S. Rocha, CNS-selective noncompetitive cholinesterase inhibitors derived from the natural piperidine alkaloid (-)-spectaline, *Eur. J. Pharmacol.* 580 (2008) 339–349. doi:10.1016/j.ejphar.2007.11.035.
- [50] L.F.N. Lemes, G. De Andrade Ramos, A.S. De Oliveira, F.M.R. Da Silva, G. De Castro Couto, M. Da Silva Boni, M.J.R. Guimarães, I.N.O. Souza, M. Bartolini,

- V. Andrisano, P.C. Do Nascimento Nogueira, E.R. Silveira, G.D. Brand, O. Soukup, J. Korábečný, N.C. Romeiro, N.G. Castro, M.L. Bolognesi, L.A.S. Romeiro, Cardanol-derived AChE inhibitors: Towards the development of dual binding derivatives for Alzheimer's disease, *Eur. J. Med. Chem.* 108 (2016) 687–700. doi:10.1016/j.ejmech.2015.12.024.
- [51] J. Cheung, M.J. Rudolph, F. Burshteyn, M.S. Cassidy, E.N. Gary, J. Love, M.C. Franklin, J.J. Height, Structures of Human Acetylcholinesterase in Complex with Pharmacologically Important Ligands, *J. Med. Chem.* 55 (2012) 10282–10286. doi:10.1021/jm300871x.
- [52] A. Inoue, T. Kawai, M. Wakita, Y. Iimura, H. Sugimoto, Y. Kawakami, The Simulated Binding of (±)-2,3-Dihydro-5,6-dimethoxy-2-[[1-(phenylmethyl)-4-piperidinyl]methyl]-1 H -inden-1-one Hydrochloride (E2020) and Related Inhibitors to Free and Acylated Acetylcholinesterases and Corresponding Structure–Activity Analyses, *J. Med. Chem.* 39 (1996) 4460–4470. doi:10.1021/jm950596e.
- [53] Y. Bourne, H.C. Kolb, Z. Radić, K.B. Sharpless, P. Taylor, P. Marchot, Freeze-frame inhibitor captures acetylcholinesterase in a unique conformation., *Proc. Natl. Acad. Sci. U. S. A.* 101 (2004) 1449–1454. doi:10.1073/pnas.0308206100.
- [54] E.H. Rydberg, B. Brumshtein, H.M. Greenblatt, D.M. Wong, D. Shaya, L.D. Williams, P.R. Carlier, Y.P. Pang, I. Silman, J.L. Sussman, Complexes of Alkylene-linked tacrine dimers with *Torpedo californica* acetylcholinesterase: Binding of bis(5)-tacrine produces a dramatic rearrangement in the active-site gorge, *J. Med. Chem.* 49 (2006) 5491–5500. doi:10.1021/jm060164b.
- [55] G. Madhavi Sastry, M. Adzhigirey, T. Day, R. Annabhimoju, W. Sherman, Protein and ligand preparation: Parameters, protocols, and influence on virtual screening enrichments, *J. Comput. Aided. Mol. Des.* 27 (2013) 221–234. doi:10.1007/s10822-013-9644-8.
- [56] M.H.M. Olsson, C.R. Søndergaard, M. Rostkowski, J.H. Jensen, PROPKA3: Consistent Treatment of Internal and Surface Residues in Empirical pK_a Predictions BT - *Journal of Chemical Theory and Computation*, *J. Chem. Theory Comput.* 7 (2011) 525–537. doi:10.1021/ct100578z.
- [57] N. Foloppe, R. Hubbard, Towards predictive ligand design with free-energy based computational methods?, *Curr. Med. Chem.* 13 (2006) 3583–3608.

doi:10.2174/092986706779026165.

- [58] J.C. Shelley, A. Cholleti, L.L. Frye, J.R. Greenwood, M.R. Timlin, M. Uchimaya, Epik: A software program for pKa prediction and protonation state generation for drug-like molecules, *J. Comput. Aided. Mol. Des.* 21 (2007) 681–691. doi:10.1007/s10822-007-9133-z.
- [59] R.A. Friesner, R.B. Murphy, M.P. Repasky, L.L. Frye, J.R. Greenwood, T.A. Halgren, P.C. Sanschagrin, D.T. Mainz, Extra Precision Glide: Docking and Scoring Incorporating a Model of Hydrophobic Enclosure for Protein-Ligand Complexes, *J Med Chem.* 49 (2006) 6177–6196. doi:10.1021/jm051256o.
- [60] T. HATANO, H. KAGAWA, T. YASUHARA, T. OKUDA, Two new flavonoids and other constituents in licorice root. Their relative astringency and radical scavenging effects., *Chem. Pharm. Bull. (Tokyo).* 36 (1988) 2090–2097. doi:10.1248/cpb.36.2090.
- [61] A. Tarozzi, F. Morroni, S. Hrelia, C. Angeloni, A. Marchesi, G. Cantelli-Forti, P. Hrelia, Neuroprotective effects of anthocyanins and their in vivo metabolites in SH-SY5Y cells, *Neurosci. Lett.* 424 (2007) 36–40. doi:10.1016/j.neulet.2007.07.017.
- [62] J. Sebastià, R. Cristòfol, M. Martín, E. Rodríguez-Farré, C. Sanfeliu, Evaluation of fluorescent dyes for measuring intracellular glutathione content in primary cultures of human neurons and neuroblastoma SH-SY5Y., *Cytometry. A.* 51 (2003) 16–25. doi:10.1002/cyto.a.10003.
- [63] A. Tarozzi, A. Merlicco, F. Morroni, F. Franco, G. Cantelli-Forti, G. Teti, M. Falconi, P. Hrelia, Cyanidin 3-O-glucopyranoside protects and rescues SH-SY5Y cells against amyloid-beta peptide-induced toxicity, *Neuroreport.* 19 (2008) 1483–1486. doi:10.1097/WNR.0b013e32830fe4b8.
- [64] A. Tarozzi, M. Bartolini, L. Piazzzi, L. Valgimigli, R. Amorati, C. Bolondi, A. Djemil, F. Mancini, V. Andrisano, A. Rampa, From the dual function lead AP2238 to AP2469, a multi-target-directed ligand for the treatment of Alzheimer's disease., *Pharmacol. Res. Perspect.* 2 (2014) e00023. doi:10.1002/prp2.23.
- [65] K.R.V. Kurapati, T. Samikkannu, V.S.R. Atluri, E. Kaftanovskaya, A. Yndart, M.P.N. Nair, β -Amyloid1-42, HIV-1Ba-L (Clade B) infection and drugs of abuse induced degeneration in human neuronal cells and protective effects of ashwagandha (*Withania somnifera*) and its constituent Withanolide A, *PLoS*

One. 9 (2014) 1–23. doi:10.1371/journal.pone.0112818.

- [66] A. Tarozzi, F. Morroni, A. Merlicco, S. Hrelia, C. Angeloni, G. Cantelli-Forti, P. Hrelia, Sulforaphane as an inducer of glutathione prevents oxidative stress-induced cell death in a dopaminergic-like neuroblastoma cell line, *J. Neurochem.* 111 (2009) 1161–1171. doi:10.1111/j.1471-4159.2009.06394.x.
- [67] H.K. Hunskaar S, The formalin test in mice - dissociation between inflammatory and noninflammatory pain., *Pain.* 30 (1987) 103–114.
- [68] A. Veloso, C. C.; Cabral, L. D. M.; Bitencourt, A. D.; Franqui, L. D.; Santa-Cecília, F. V.; Dias, D. F.; Soncini, R. Vilela, F. C.; Giusti-Paiva, Anti-inflammatory and antinociceptive effects of the hydroethanolic extract of the flowers of *Pyrostegia venusta* in mice, *Rev. Bras.* 22 (2012) 162–168. http://www.scielo.br/scielo.php?pid=S0102695X2012000100024&script=sci_arttext.
- [69] F.Q. Cunha, G.E. Souza, C. a Souza, B.C. Cerqueira, S.H. Ferreira, In-vivo blockage of neutrophil migration by LPS is mimicked by a factor released from LPS-stimulated macrophages., *Br. J. Exp. Pathol.* 70 (1989) 1–8. <http://www.ncbi.nlm.nih.gov/pubmed/2647118>.
- [70] S.R. Chaplan, F.W. Bach, J.W. Pogrel, J.M. Chung, T.L. Yaksh, Quantitative assessment of tactile allodynia in the rat paw, *J. Neurosci. Methods.* 53 (1994) 55–63. doi:10.1016/0165-0270(94)90144-9.
- [71] L. Levy, Carrageenan paw edema in the mouse, *Life Sci.* 8 (1969) 601–606. doi:10.1016/0024-3205(69)90021-6.
- [72] E. Ricciotti, G.A. FitzGerald, Prostaglandins and Inflammation, *Arterioscler. Thromb. Vasc. Biol.* 31 (2011) 986–1000. doi:10.1161/ATVBAHA.110.207449.
- [73] C.J. Smith, Y. Zhang, C.M. Koboldt, J. Muhammad, B.S. Zweifel, A. Shaffer, J.J. Talley, J.L. Masferrer, K. Seibert, P.C. Isakson, Pharmacological analysis of cyclooxygenase-1 in inflammation, *Proc. Natl. Acad. Sci.* 95 (1998) 13313–13318. doi:10.1073/pnas.95.22.13313.

ABBREVIATION

AD	Alzheimer Disease
Aβ	β -Amyloid
ACh	Acetylcholine
AChE	Acetylcholinesterase
APP	Amyloid precursor protein
COX	Ciclooxigenase

DCFDA	2',7'-dichlorodihydrofluorescein diacetate
GSH	Glutathione
LOX	Lipoxygenase
LPS	Lipopolysaccharide
MCB	Monochlorobimane
MTDL	Multi-Target-Direct-Ligant
ROS	Reactive oxygen species
SAR	Structure–activity relationship

Table 1. Cholinesterase inhibitory activity, DPPH scavenging capacity, neurotoxic and direct antioxidant effects in neuron cells of compounds **12a-n**

Compounds	Cholinesterase		DPPH	Neuron	Neurotoxicity
	inhibitor IC ₅₀ (μM) ^a		scavenging	Antioxidant	IC ₅₀ (μM) ^d
	EeAChE	eqBuChE	EC ₅₀ (μM) ^b	effects IC ₅₀ (μM) ^c	
12a	0.46 (3)	24.97 (2)	49.41	16.87	n.d. ^f (6%) ^g
12b	16.74 (3)	-	46.66	25.94	n.d. (9%)
12c	>30	-	45.38	n.d. ^e	n.d. (28%)
12d	> 30	-	73.77	-	-
12e	> 30	-	78.09	-	-
12f	> 30	-	> 100	-	-
12g	> 30	-	> 100	-	-
12h	> 30	-	> 100	-	-
12i	> 30	-	> 100	-	-
12j	> 30	-	> 100	-	-
12k	> 30	-	20.47	-	-
12l	> 30	-	> 100	-	-
12m	> 30.00	-	12.45	-	-
12n	> 30.00	-	> 100	-	-
Donepezil	0.026 (2)	4.69 (2)	-	n.d.	-
Curcumin	132.13 (3)	>300 (2)	-	-	-
Trolox	-	-	04.86	-	-
ferulic acid	-	-	35.54	11.82	-
iso-ferulic acid	-	-	> 100	-	-

^a The IC₅₀ are geometric means from the number of independent experiments indicated in parenthesis; each was performed in triplicate.

^b Antioxidant activity are shown as EC₅₀ values in μM concentrations. All compounds were analyzed in triplicate and the results expressed as average

^c Concentration of compound resulting in 50% inhibition of ROS formation induced by H₂O₂ (100 μM) in neuronal SH-SY5Y cells. The values are mean of at least two independent experiments;

^d Concentration of compound resulting in 50% inhibition of neuronal viability after 24 h treatment;

^e n.d: IC₅₀ not determined because less than 50% inhibition of ROS formation induced by H₂O₂ in neuronal SH-SY5Y cells was observed at the highest concentration tested (40 μM);

^f n.d: IC₅₀ not determined because less than 50% inhibition of neuronal viability was observed at the highest concentration tested (40 μM);

^g Values in parenthesis are percent inhibition of neuronal viability observed at highest tested concentration (40 μM).

Table 2. Docking scores of the compounds **12a**, **12b**, **12c** and donepezil (used as reference) provided by docking with Glide in the Extra Precision Mode.

Compound	Free AChE	Acetylated AChE	Michaelis Complex
12^a	-16.129	-16.956	-11.567
12b	-15.586	-15.982	-9.961
12c	-13.913	-16.566	-11.463
Donepezil	-15.469	-15.862	-11.757

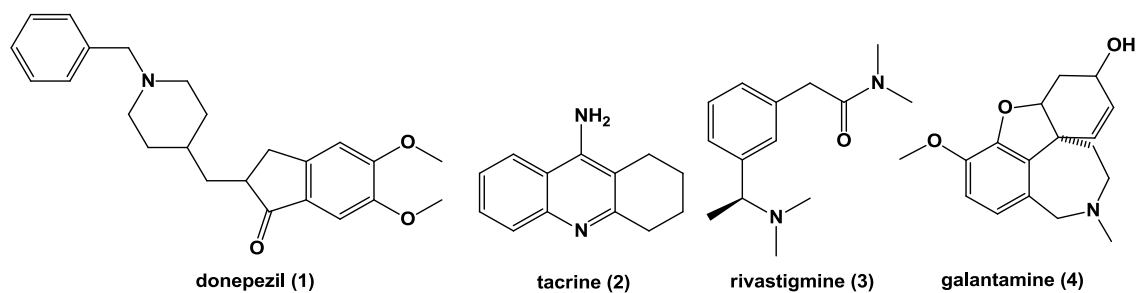


Fig. 1. Chemical structures of AChE inhibitors currently used in the treatment of AD

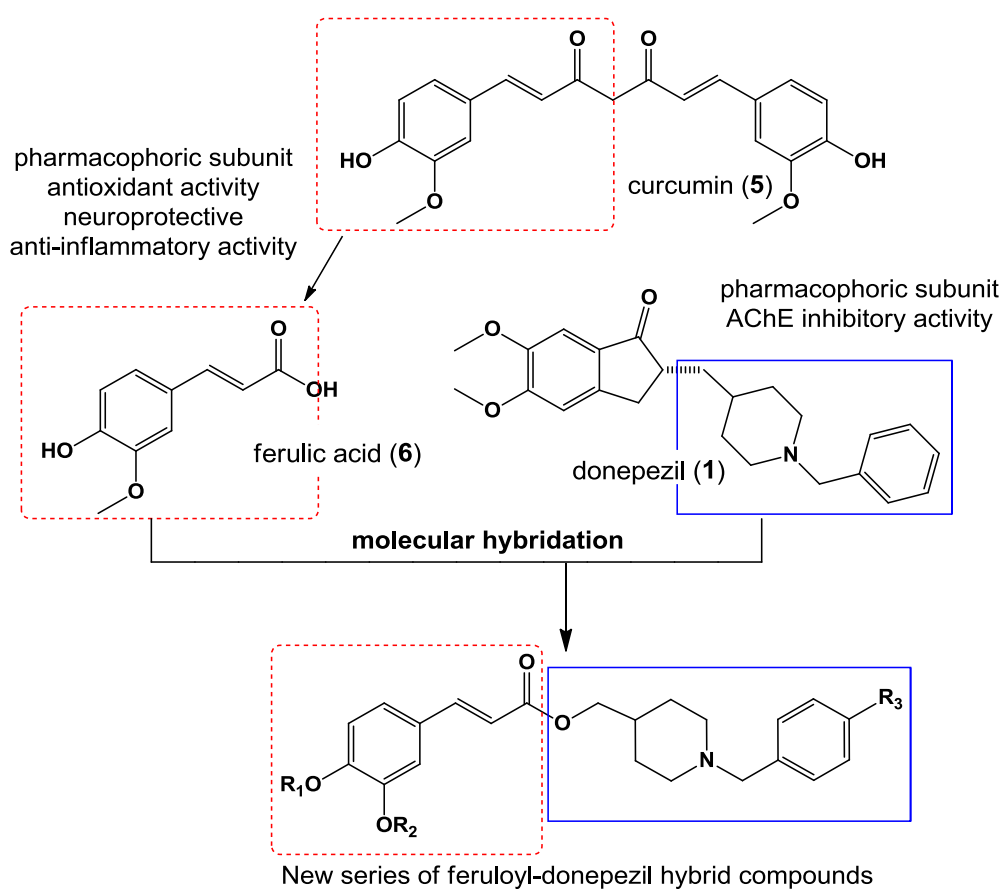


Fig. 2. Design strategy for a new series of feruloyl-donepezil hybrid compounds

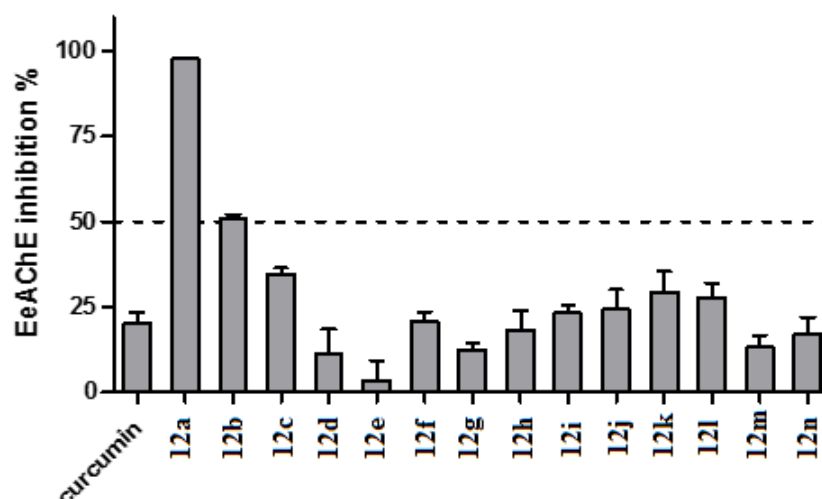


Fig. 3. Screening of feruloyl-donepezil hybrids (**12a-12n**) for EeAChE inhibition. The compounds were pre-incubated for 10 min with the enzyme and reaction was followed for 5 min and activity (velocity) was expressed as percent of control (vehicle). Data are means and pooled SD from 2-4 experiments, each performed in triplicate.

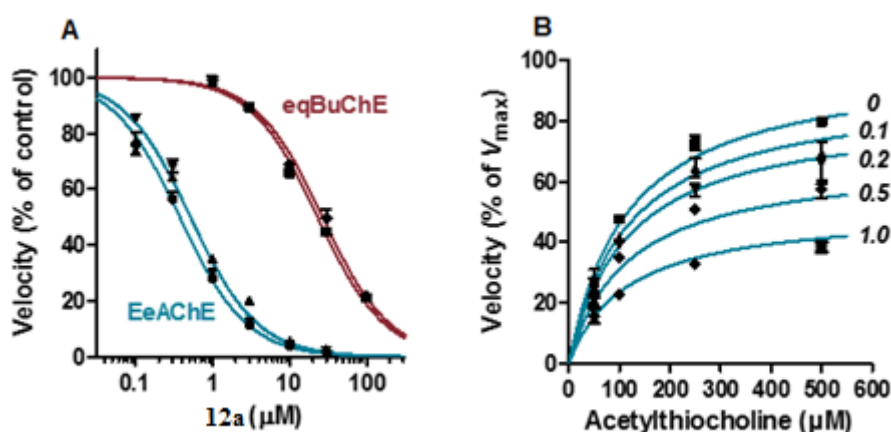


Fig. 4. Inhibition curves and mechanism of inhibition of **12a**. **A.** Concentration-dependent inhibition of EeAChE and eqBuChE by **12a**. Independent experiments are shown in different symbols, which are mean \pm SD of triplicates; fitted curve parameters are shown in Table 2. **B.** Substrate competition data for EeAChE and best-fitting model (simple linear non-competitive inhibition). The concentration of **12a** (μM) is indicated to the right of each curve. Data are pooled from two experiments, each performed in triplicate.

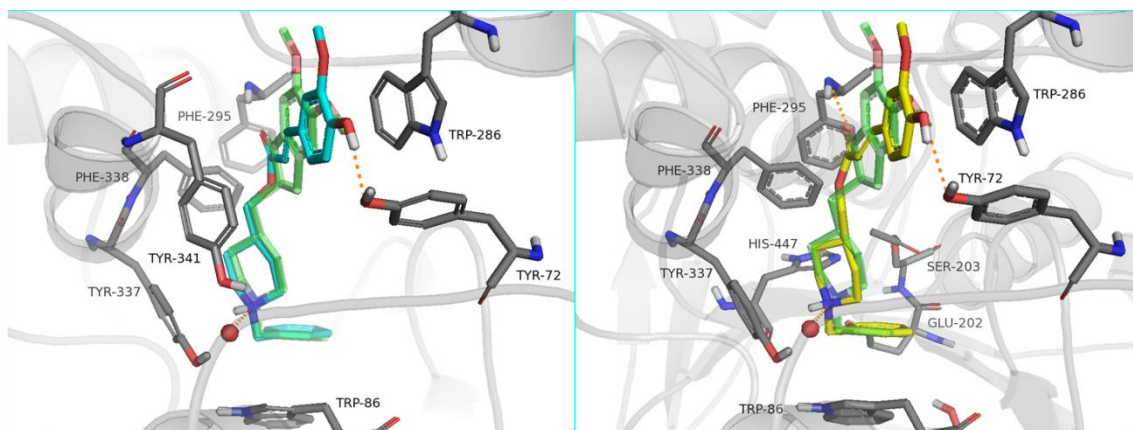


Fig. 5. Docking results for **12a** in the free (light blue) and acetylated (yellow) states, superposed with the experimental binding mode of donepezil (transparent green). W931 is represented as a red sphere and the hydrogen bonds are highlighted as orange dashed lines.

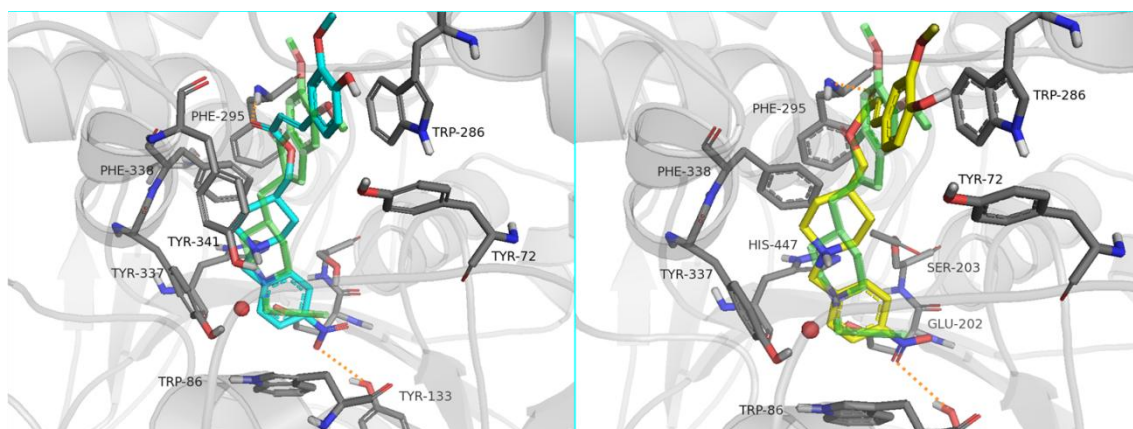


Fig. 6. Docking results for **12b** in the free (light blue) and acetylated (yellow) states, superposed with the experimental binding mode of donepezil (transparent green). W931 is represented as a red sphere and the hydrogen bonds are highlighted as orange dashed lines.

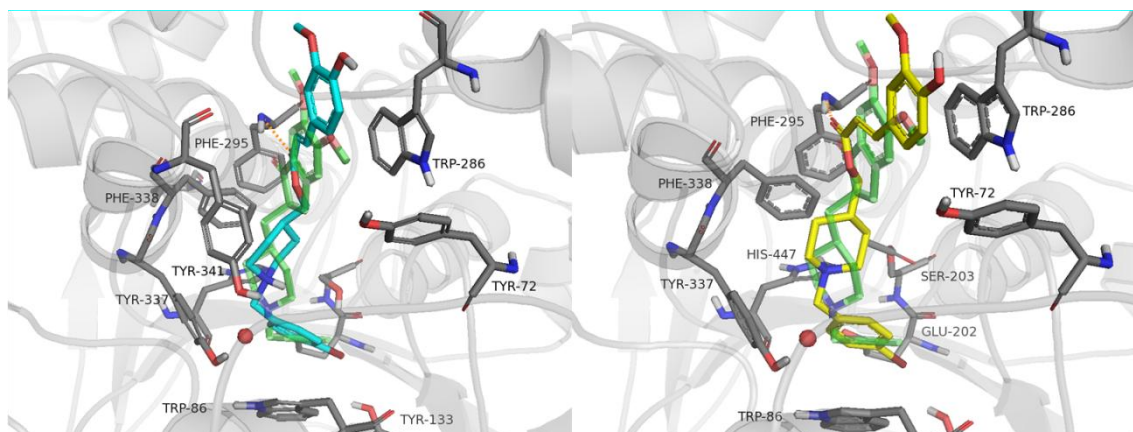


Fig. 7. Docking results for **12c** in the (A) free (light blue) and acetylated (yellow) states, superposed with the experimental binding mode of donepezil (transparent green). W931 is represented as a red sphere and the hydrogen bonds are highlighted as orange dashed lines.

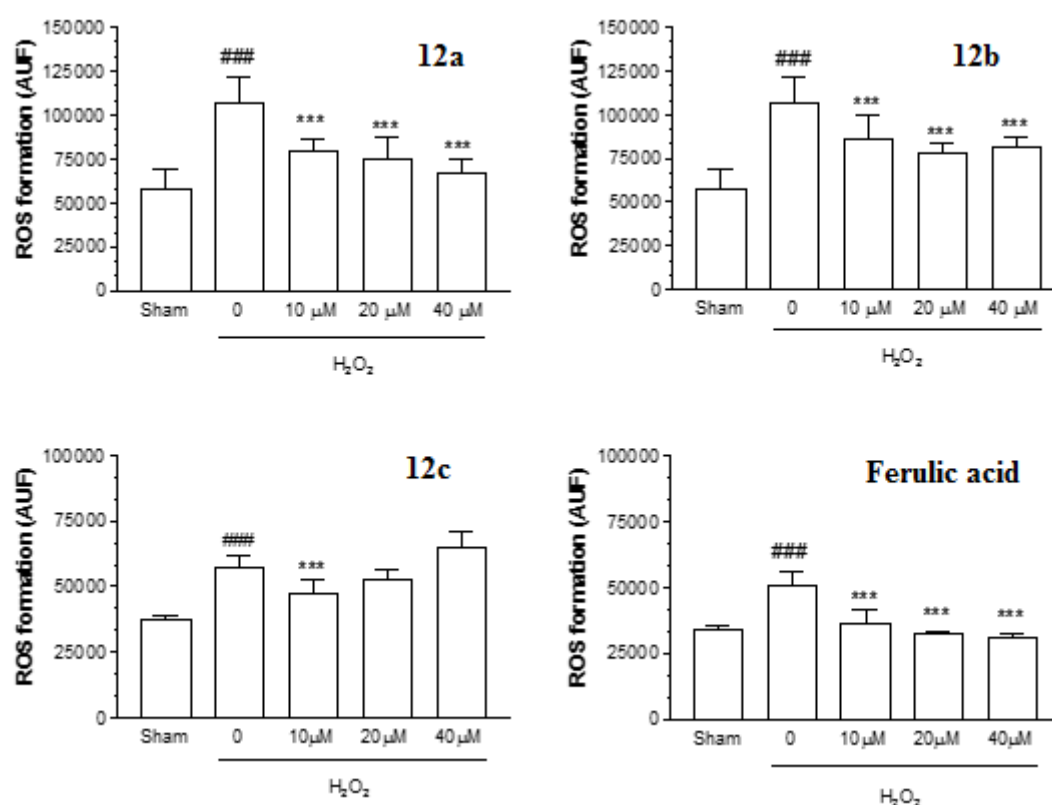


Fig. 8. Compounds **12a**, **12b**, **12c** and ferulic acid counteract the ROS formation induced by H_2O_2 in neuronal SH-SY5Y cells. The cells were treated with various concentrations of compounds and H_2O_2 (100 μ M) for 30 min. At the end of the treatment, intracellular ROS formation was determined using DCFDA probe (as described in the experimental section). The arbitrary units of fluorescence (AUF) values are shown as mean \pm SD of three independent experiments (### p <0.001 vs sham; *** p <0.001 vs treated with H_2O_2).

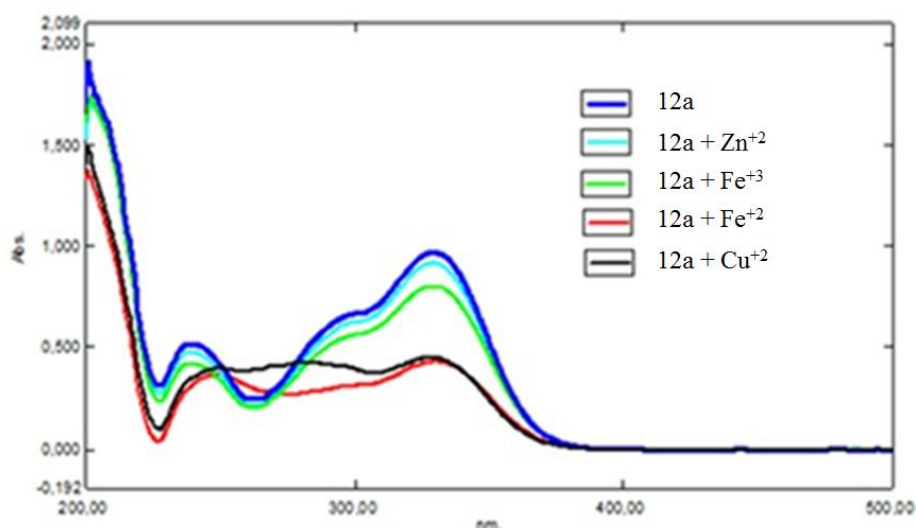


Fig.9. UV-absorbance spectra of **12a** alone or in the presence of ZnCl_2 , FeSO_4 , FeCl_3 and CuSO_4 .

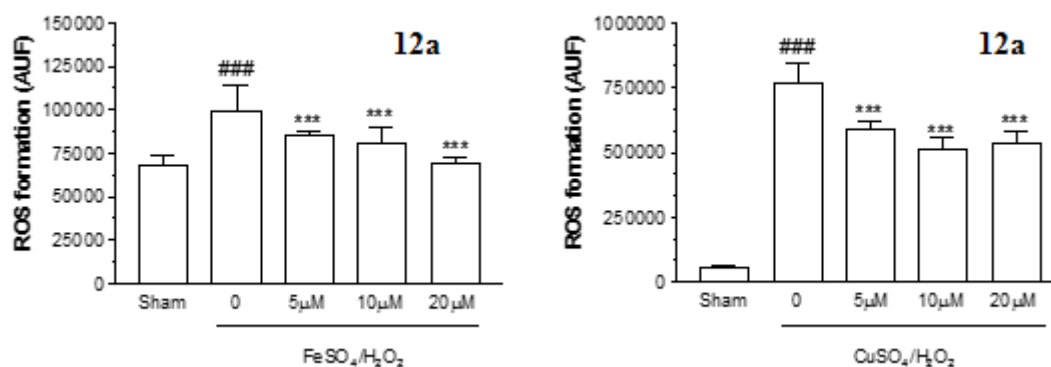


Fig.10. Compound **12a** counteracted the ROS formation induced by either $\text{FeSO}_4/\text{H}_2\text{O}_2$ or $\text{CuSO}_4/\text{H}_2\text{O}_2$ in neuronal SH-SY5Y cells. The cells were treated with various concentrations of compound **12a** and either $\text{FeSO}_4/\text{H}_2\text{O}_2$ or $\text{CuSO}_4/\text{H}_2\text{O}_2$ (25 μM /100 μM) for 30 min. At the end of the treatment, intracellular ROS formation was determined using DCFDA probe (as described in the experimental section). The arbitrary units of fluorescence (AUF) values are shown as mean \pm SD of three independent experiments (### p <0.001 vs sham; *** p <0.001 vs treated with either $\text{FeSO}_4/\text{H}_2\text{O}_2$ or $\text{CuSO}_4/\text{H}_2\text{O}_2$).

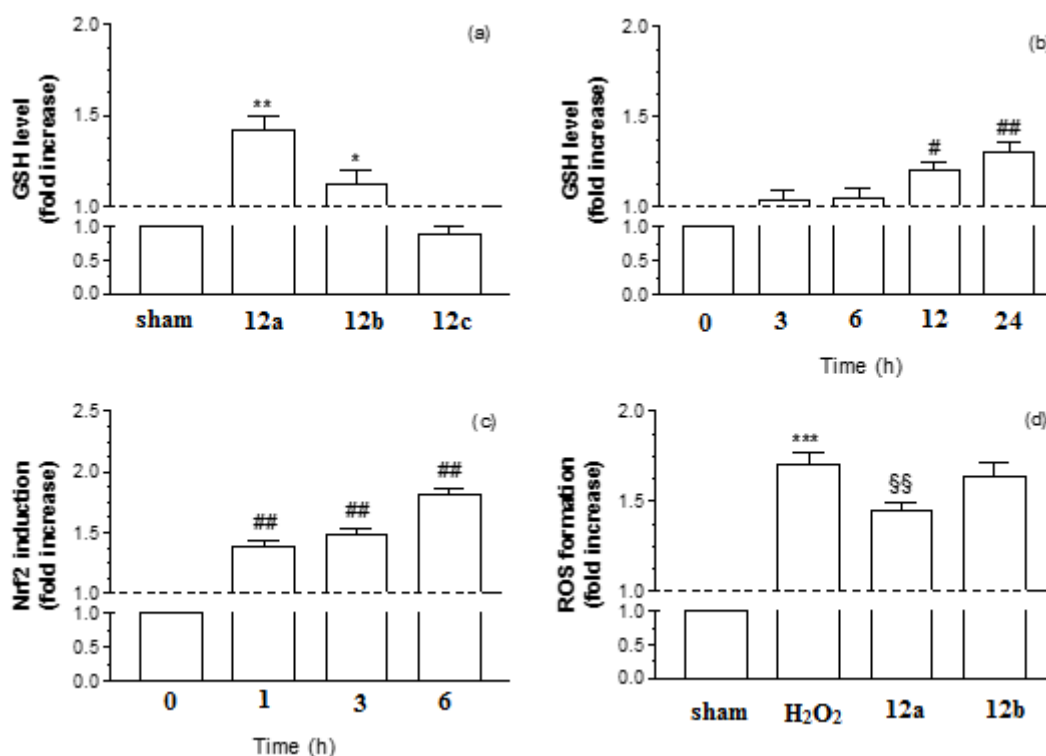


Fig. 11. Compound **12a** increases cytosolic GSH and nuclear Nrf2 levels as well as indirect antioxidant effects in neuronal SH-SY5Y cells. The cells were treated with 20 μ M of compounds **12a**, **12b**, **12c** for 24 h (a) or various increasing treatment time (b, c). At the end of the treatment, cytosolic GSH and nuclear Nrf2 levels were determined using MCB probe and immunoassay, respectively (as described in experimental section). (d) After the 24 h treatment with 20 μ M of compound **12a**, the cells were also treated with H₂O₂ (100 μ M, 30 min) to evaluate the intracellular ROS formation using DCFDA probe (as described in the experimental section) in SH-SY5Y cells. The results are expressed as a percentage of control cells. The values are reported as mean \pm SD of three independent experiments (* p <0.05, ** p <0.01, *** p <0.001 vs sham; # p <0.05, ## p <0.01 vs untreated; §§ p <0.01 vs treated with H₂O₂).

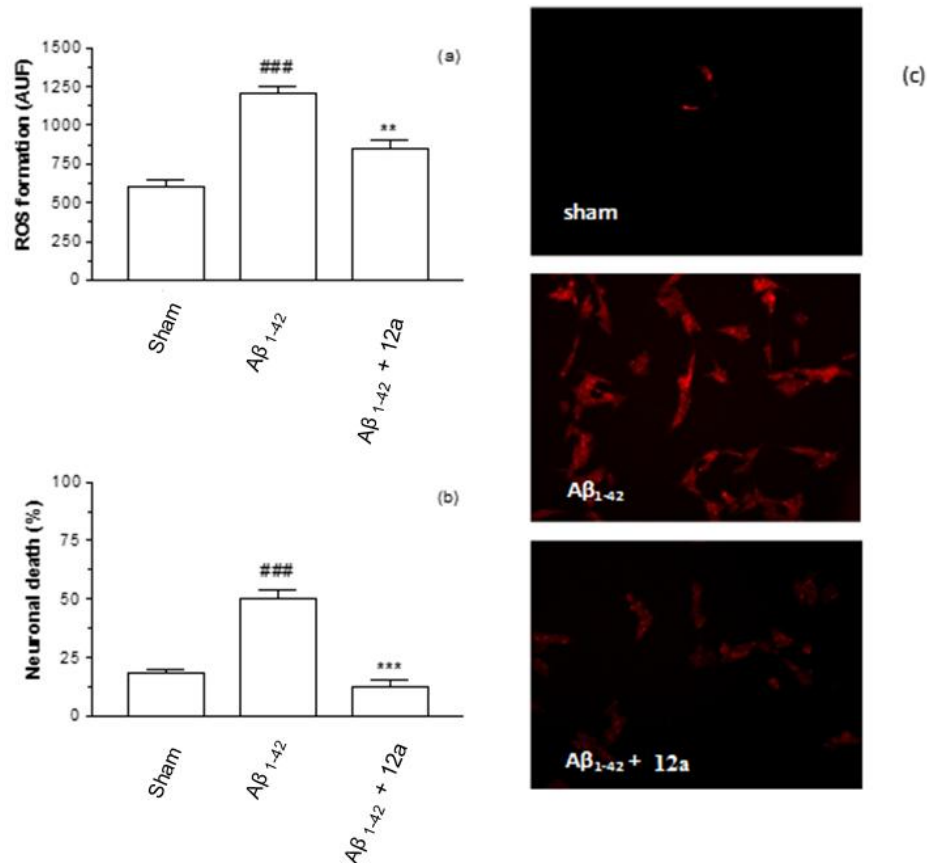


Fig. 12. Compound **12a** counteracts ROS formation and neuronal death induced by Aβ₁₋₄₂ oligomers in neuronal SH-SY5Y cells. The cells were treated with 20 μM of compound **12a** and Aβ₁₋₄₂ oligomers (20 μM) for either 4 h (a) or 24 h (b). At the end of the treatment, intracellular ROS formation and neuronal death were determined using DCFDA and propidium iodide probe (as described in the experimental section). (c) Representative images of ROS formation. The results are expressed as a percentage of control cells. The values are reported as mean ± SD of three independent experiments (###p<0.001 vs sham; **p<0.01, ***p<0.001 vs treated with Aβ₁₋₄₂ oligomers).

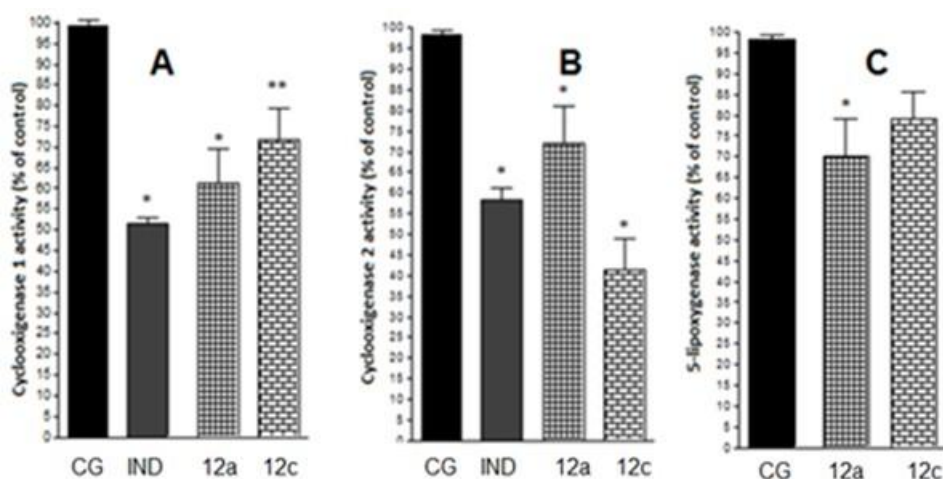


Fig. 13. Effect of compounds **12a** and **12c** on COX-1, COX-2 and 5-LOX activity in mice treated with carrageenan (CG). Mice were treated with compounds **12a**, **12c** (100 $\mu\text{mol/kg}$, p.o) and indomethacin (IND, 100 $\mu\text{mol/kg}$, p.o.) 1 h before intraplantar injection of carrageenan (400 $\mu\text{g/paw}$). After 3 h, the COX-1, COX-2 and 5-LOX activity was determined as reported in the Experimental section. Values are expressed as mean \pm SEM (n=8) in terms of enzymatic activity percentage (* $P < 0.05$ compared to the carrageenan group; ** $P < 0.01$ compared to the carrageenan group and the indomethacin group).

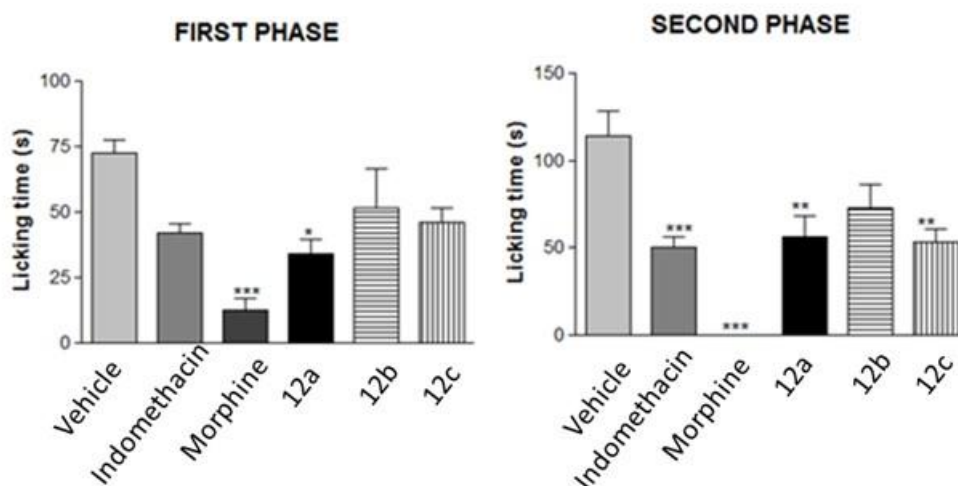


Fig. 14. Effect of compounds **12a**, **12b** and **12c** in a mice model of formalin-induced inflammatory pain. Mice were pre-treated orally with vehicle, compounds **12a-c** (100 $\mu\text{mol/kg}$), indomethacin (100 $\mu\text{mol/kg}$), morphine (39 $\mu\text{mol/kg}$) or vehicle (saline + DMSO 2%) prior to formalin administration. The total time spent licking the hindpaw was measured in the first and

second phases after intraplantar injection of formalin. Values are expressed as mean \pm SEM (n=8) (*p<0.05, **p<0.01, and ***p<0.001 compared to control group).

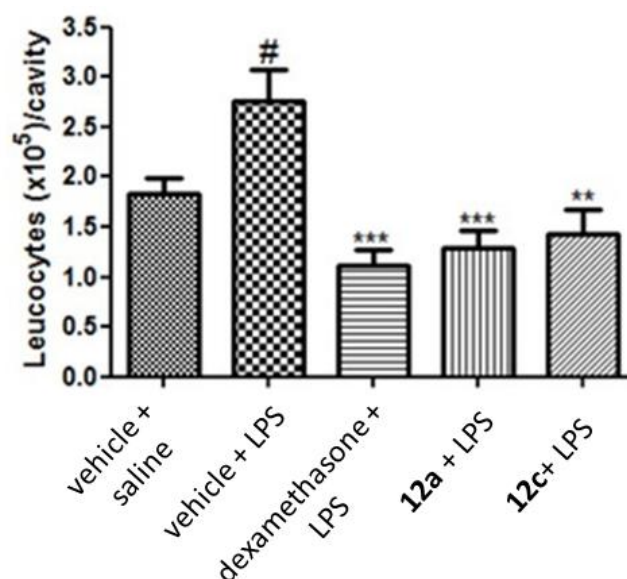


Fig. 15. Effect of compounds **12a** and **12c** in a mouse model of LPS-induced peritonitis. Mice were pre-treated orally with compounds **12a** and **12c** (100 μ mol/kg), dexamethasone (10 mg/kg, p.o.) or vehicle (saline + DMSO 2%) prior to LPS administration. The number of leukocytes recruited in the peritoneal cavity was determined. Values are expressed as mean \pm SEM (n=8). #P<0.05 compared with the saline + vehicle group; ***P<0.01, **P<0.01 and *P<0.05 compared with the vehicle + LPS group.

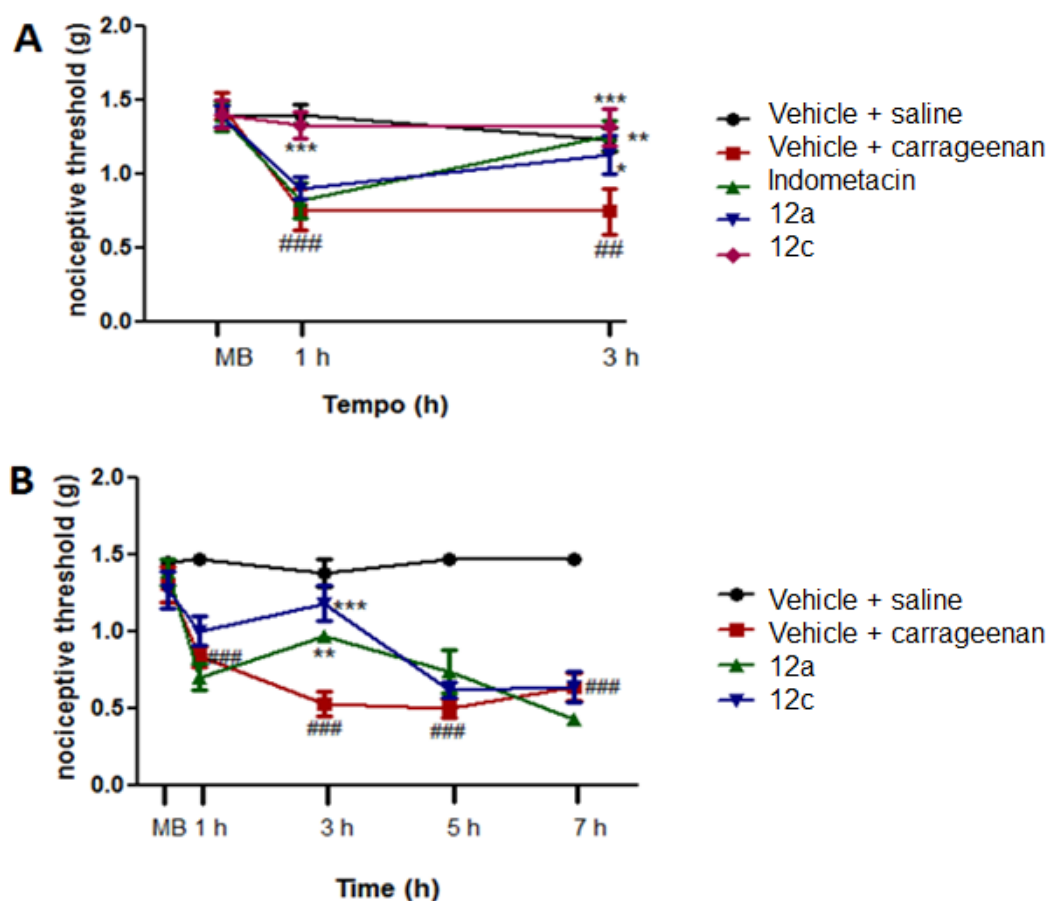


Fig. 16. Effect of compounds **12a** and **12c** on mechanical hyperalgesia in a mice model of carrageenan-induced paw edema. Mice were pre-treated orally with compounds **12a** and **12c** (100 $\mu\text{mol/kg}$ p.o) or indomethacin (100 $\mu\text{mol/kg}$ p.o) prior to intraplantar injection of carrageenan (100 $\mu\text{g/paw}$). The results are presented as threshold for touch sensitivity (weight in grams). Values are expressed as mean \pm SEM (n=8). ### P<0.01 compared with the saline + vehicle group; *** P<0.01, ** P<0.01 and * P<0.05 compared with the vehicle + carrageenan group.

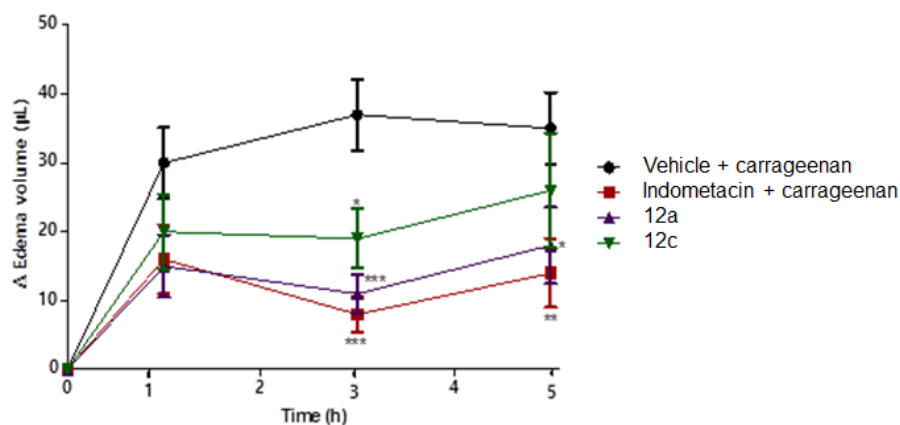
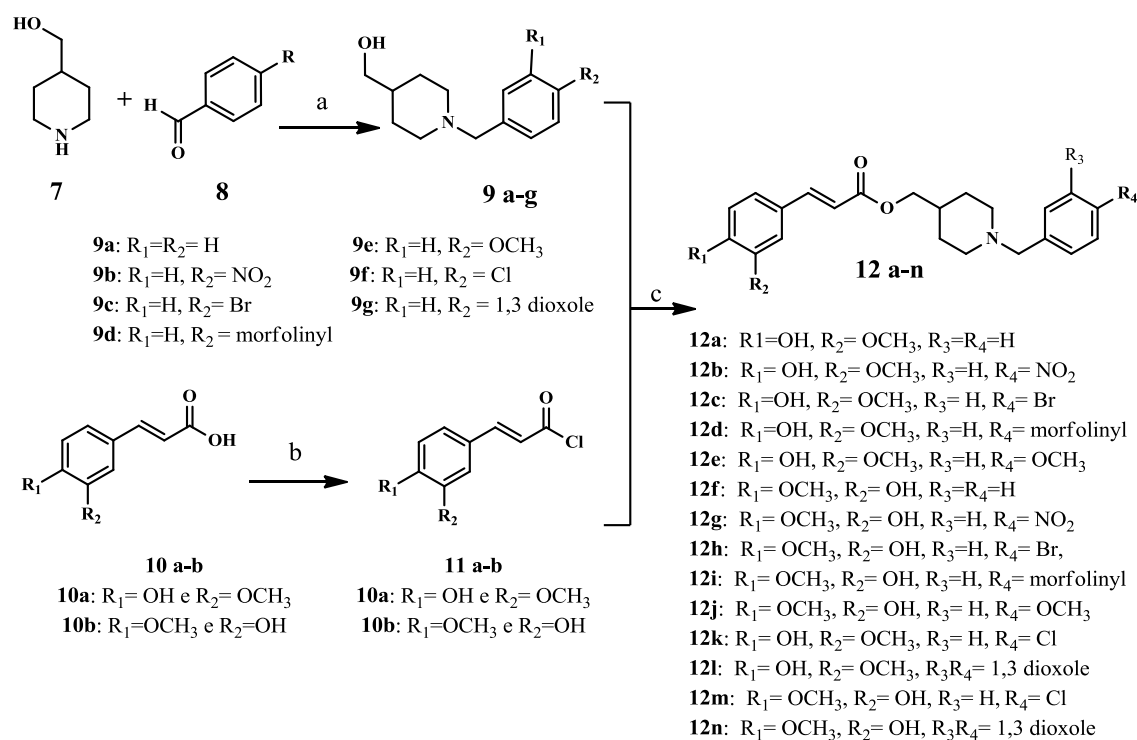


Fig. 17. Effect of compounds **12a** and **12c** in a mouse model of carrageenan-induced paw edema. Mice were pre-treated orally with compounds **12a** and **12c** (100 $\mu\text{mol/kg}$ p.o) or indomethacin (100 $\mu\text{mol/kg}$ p.o) prior to intraplantar injection of carrageenan (Cg, 100 $\mu\text{g/paw}$). The results are presented as the paw volume (μL) variation in relation to the basal values. Values are expressed as mean \pm SEM (n=8). *P<0.05, **P<0.01, ***P<0.001 compared with control group.

Figure(s)



Scheme 1. Reagents and conditions: (a) $NaBH_3CN$, $ZnCl_2$, MeOH, rt, 72 h, 70-87%; (b) $SOCl_2$, DMF, CH_2Cl_2 , N_2 , 1h, 98%; (c) CH_2Cl_2 , N_2 , 15 min, rt, 55-70%